Predicting OH stretching fundamental wavenumbers of alcohols for conformational assignment: different correction patterns for density functional and wave-function-based methods

-

Electronic Supplementary Information

Robert Medel* and Martin A. Suhm

Contents

*Institute of Physical Chemistry, University of Goettingen, Tammannstr. 6, 37077 Goettingen. Germany. E-mail: rmedel@gwdg.de, msuhm@gwdg.de

1 Evaluation of additional alcohols in the test set

1.1 Cyclohexanol

Cyclohexanol is a secondary alcohol with two conformational degrees of freedom: torsion around the C−O bond and ring inversion. Neglecting non-chair ring conformations, this leads to four diasteromeric conformers, in sequence of increasing predicted energy: equatorial-*gauche* (E*g*), equatorial-*trans* (E*t*), axial-*gauche* (A*g*) and axial-*trans* (A*t*). Their structures and relevant properties at PBE0-D3 level are presented in Fig. S1.

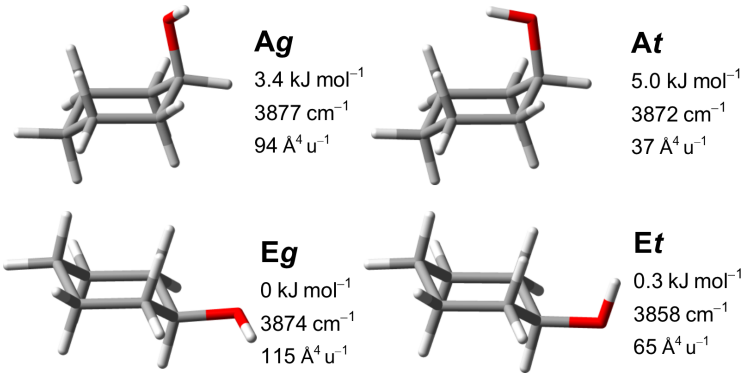

Figure S1: Predicted conformers of cyclohexanol with respective harmonically zero-point-corrected relative energy, uncorrected harmonic OH stretching wavenumber and Raman activity obtained at PBE0-D3 level. For B3LYP-D3 and SCS-LMP2 results see Table S18. The *g* conformers have an enantiomeric degeneracy.

Even though the axial conformers are predicted to be high in energy, a large fraction of their cumulative room temperature population might survive in a jet expansion due to the very high barriers for the ring inversion, which were calculated in the 40–50 kJ mol^{-1} range.[1,2] In recent studies with rotational spectroscopy no monomeric axial conformer could be detected under jet conditions,[2,3] while in contrast four of six detected dimer structures were found to feature one axial conformer as a constituent.[2] For the simulation of the spectrum (Fig. S2) we assume that the total axial population at 298 K is preserved (estimated from PBE0-D3 Gibbs energies as 17%), while the respective *gauche*/*trans* ratios relax to 100 K.

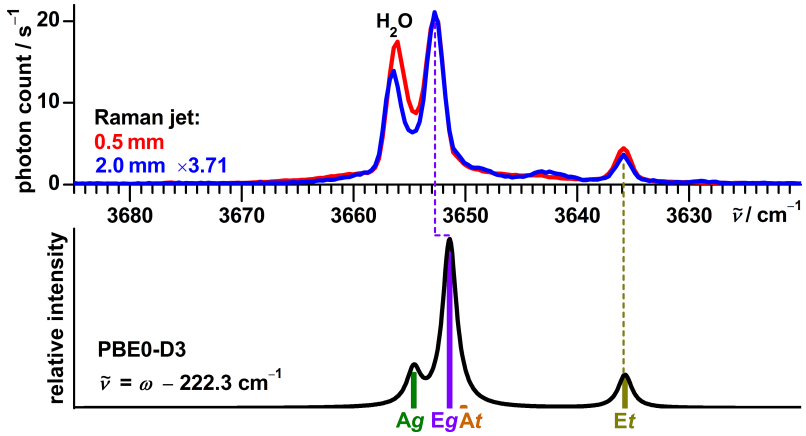

Figure S2: Raman jet spectra[4] of cyclohexanol at two detection distances from the nozzle scaled to similar intensities of the 3653 cm^{-1} signal, in comparison with a simulated spectrum. For the simulation the PBE0-D3 harmonic wavenumbers are corrected as proposed by our model and a Lorentzian broadening of FWHM = 1.5 cm^{-1} applied. For the intensities a Boltzmann distribution at 100 K between *g* and *t* conformers and a preserved E/A ratio of 83/17 (calculated for 298 K) is assumed.

In the experimental spectrum[4] at 0.5 mm detection distance from the nozzle (Fig. S2) two intense signals at 3656 and 3653 cm^{-1} are present as well as a third signal of medium intensity at 3636 cm^{-1}. Based on the positions predicted by our model (Table S1) we assign the band at 3653 cm^{-1} to the Eg and the band at 3636 cm^{-1} to the Et conformer. This is in accordance with previous assignments at 3652 and 3636 cm^{-1} for an infrared spectrum of the vapor at 100 °C.[5]

Table S1: Assignments, experimental band positions and deviations of the predictions for the OH-stretching fundamentals of conformers of cyclohexanol

conformer	method	$\tilde{\nu}$/ cm^{-1}	$(\omega + \kappa - \tilde{\nu}_{exp})$/ cm^{-1}
Eg	experiment	3653	
Eg	B3LYP-D3	3650	−3
Eg	PBE0-D3	3651	−2
Eg	SCS-LMP2	3654	1
Et	experiment	3636	
Et	B3LYP-D3	3636	0
Et	PBE0-D3	3636	0
Et	SCS-LMP2	3637	1
Ag	experiment	not observed	
Ag	B3LYP-D3	3655	
Ag	PBE0-D3	3655	
Ag	SCS-LMP2	3656	
At	experiment	not observed	
At	B3LYP-D3	3656	
At	PBE0-D3	3650	
At	SCS-LMP2	3658	

When increasing the detection distance from the nozzle to 2.0 mm the signals at 3636 cm^{-1} and 3656 cm^{-1} lose in relative intensity in the colder part of the expansion. This is expected from a further relaxation of the Et into the Eg conformer. The predictions suggest an assignment of the band at 3656 cm^{-1} to the Ag conformer; however, the observed relative intensity is higher than expected. The most likely reason is a significant contribution from the symmetric stretch fundamental of a water impurity, which is known to scatter at this Stokes shift.[6] Telling is the slight upshift in the colder part of the expansion, attributed to rotational cooling, as it is also visible for the water impurity in spectra of other compounds investigated in this work (Fig. 8 in the main document and Fig. S4). Due to this spectral coincidence we can neither establish nor exclude the presence of axial cyclohexanol under jet conditions. We plan to revisit this question in the future. Another possible explanation for the doublet signal – a resolved spectral splitting due to tunneling similar to propargyl alcohol – is very unlikely, since the ground state splitting of Eg was determined[3] to be only hc 1.7 cm^{-1} and would need to increase by hc 3 cm^{-1} upon OH stretch excitation.

In the colder part of the expansion additional bands between 3540–3490 cm^{-1} increase in intensity, which we assign as the donor signals of a multitude of dimers.[2,7] They are accompanied by acceptor signals at 3643 and 3629 cm^{-1}. The spectra in the full monochromator range (3700–3240 cm^{-1}) is shown in Fig S22.

1.2 (−)-Isopinocampheol

(−)-Isopinocampheol, or (1*R*,2*R*,3*R*,5*S*)-2,6,6-trimethylbicyclo[3.1.1]heptan-3-ol, is a secondary alcohol and a constitutional isomer of (−)-borneol with a different bridging of the rings (compare Fig. S3 with Fig. 7 in the main document). The bicyclo[3.1.1]heptane carbon backbone of isopinocampheol is less rigid than the bicyclo[2.2.1]heptane frame of borneol. Depending on the substitution, the two interconnected six-membered rings adopt conformations in the continuum between boat/chair, half-chair/half-chair and chair/boat.[8] For the carbon frame of isopinocampheol we find computationally a single minimum close to the half-chair/half-chair conformation with the alpha carbon atom slightly deflected out of the plane in the direction of the quaternary carbon atom, in agreement with the result of an NMR study.[8] This limits the relevant conformational space to the torsion around the C−O bond, which leads to three diastereomeric conformers (Fig. S3) similar to borneol. The change in the carbon frame is predicted to induce substantial downshifts in all conformers while preserving their spectral sequence.

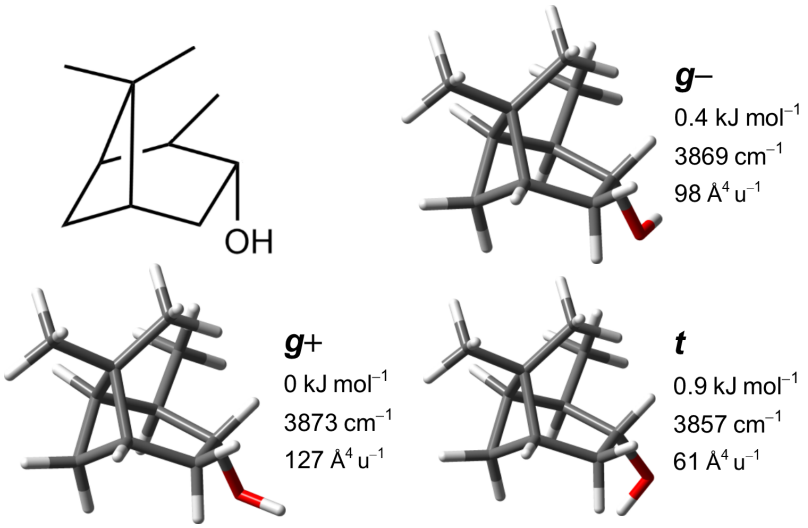

Figure S3: Strucutural formula and predicted conformers of (−)-isopinocampheol with respective harmonically zero-point-corrected relative energy, uncorrected harmonic OH stretching wavenumber and Raman activity obtained at PBE0-D3 level. For B3LYP-D3 and SCS-LMP2 results see Table S20.

In a previous FTIR jet study[9,10] we have observed a band with a maximum at 3648 cm^{-1}, assigned to *g*+ (part of the training set), and a shoulder at 3644 cm^{-1}. In the Raman jet spectra (Fig. S4) this is now resolved as two bands at 3649 and 3644 cm^{-1}, with the latter newly assigned to *g*−. Additional bands at 3632 and 3656 cm^{-1} are assigned to the *t* conformer respectively a water impurity (Table S2).

The intensity ratio 3649/3644 increases only very slightly when probing a colder part of the expansion. This indicates a smaller energy difference between the *gauche* conformers of isopinocampheol compared to those of borneol, in agreement with the predictions of B3LYP-D3 ($0.9 \rightarrow 0.4\,kJ\,mol^{-1}$) and PBE0-D3 ($1.0 \rightarrow 0.4\,kJ\,mol^{-1}$), but not with those of SCS-LMP2 ($0.1 \rightarrow 0.8\,kJ\,mol^{-1}$). Due to the very low vapor pressure of isopinocampheol (about 4 Pa)[11] no bands assignable to clusters are observed (Fig. S24).

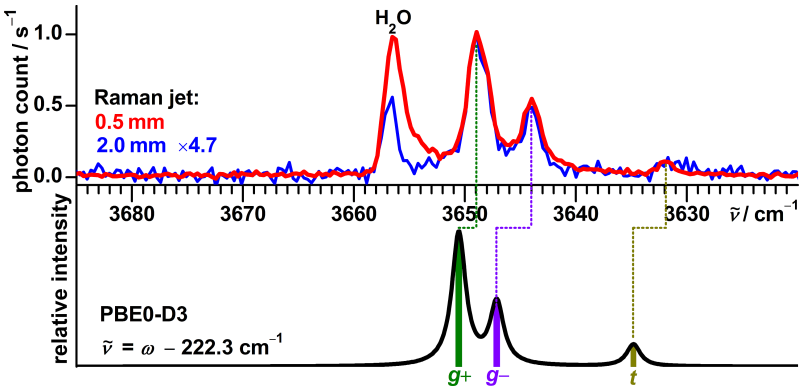

Figure S4: Raman jet spectra of (−)-isopinocampheol at two detection distances from the nozzle scaled to similar intensities of the 3649 cm^{-1} signal, in comparison with a simulated spectrum. For the simulation the PBE0-D3 harmonic wavenumbers are corrected as proposed by our model and a Lorentzian broadening of FWHM = 1.5 cm^{-1} is applied. A Boltzmann distribution at 100 K is assumed.

Table S2: Assignments, experimental band positions and deviations of the predictions for the OH-stretching fundamentals of conformers of (−)-isopinocampheol

conformer	method	$\tilde{\nu}$/ cm^{-1}	$(\omega + \kappa - \tilde{\nu}_{\mathrm{exp}})$/ cm^{-1}
$g+$	experiment	3649	
$g+$	B3LYP-D3	3649	0
$g+$	PBE0-D3	3651	2
$g+$	SCS-LMP2	3647	−2
$g-$	experiment	3644	
$g-$	B3LYP-D3	3647	3
$g-$	PBE0-D3	3647	3
$g-$	SCS-LMP2	3645	1
t	experiment	3632	
t	B3LYP-D3	3636	4
t	PBE0-D3	3635	3
t	SCS-LMP2	3636	4

2 Overview of the alcohol conformers in the data set

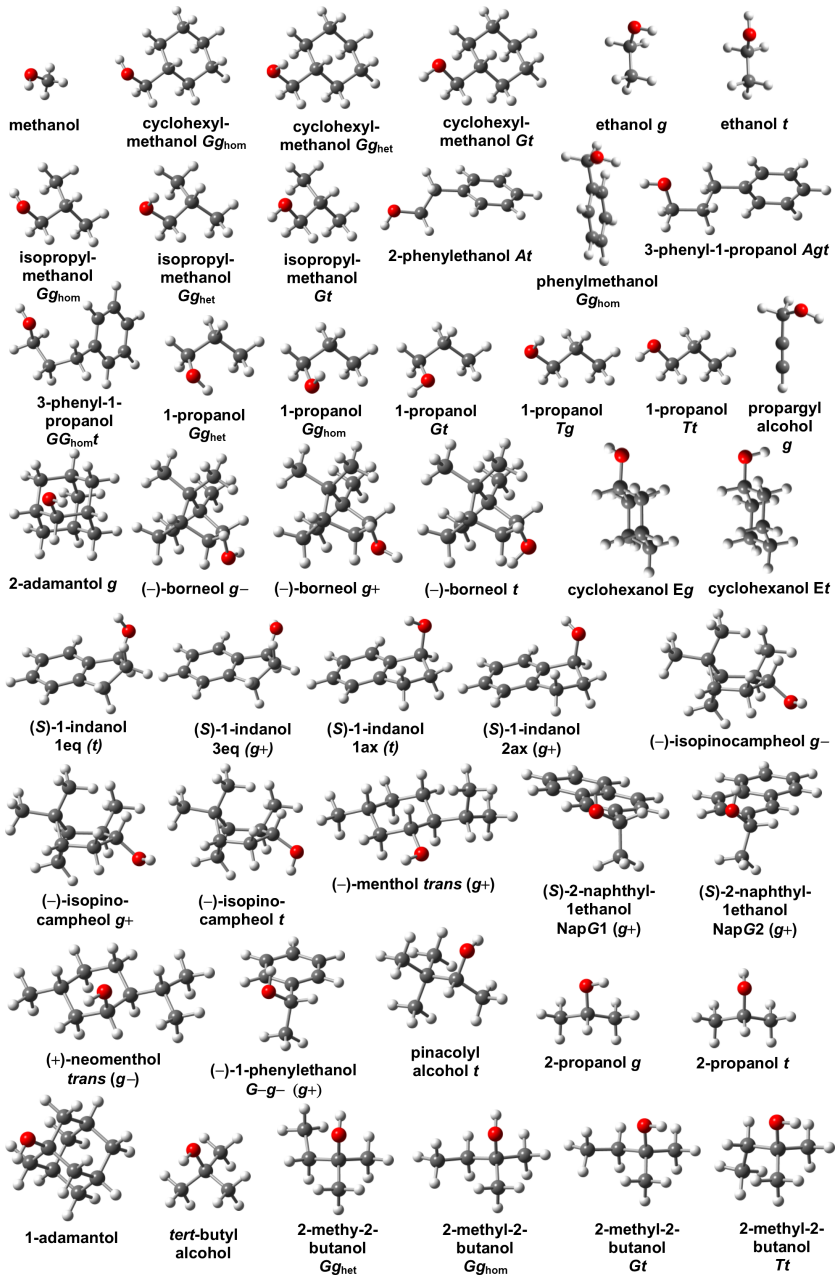

Figure S5: Structures of all alcohols conformers in the combined training/test data set optimized at PBE0-D3 level. For 1-indanol, menthol, 2-naphthyl-1-ethanol, neomenthol and 1-phenylethanol the arrangement of the HOCH dihedral is added in parentheses to the literature label.

3 Updated correlation graphs and corrections for protiated alcohols

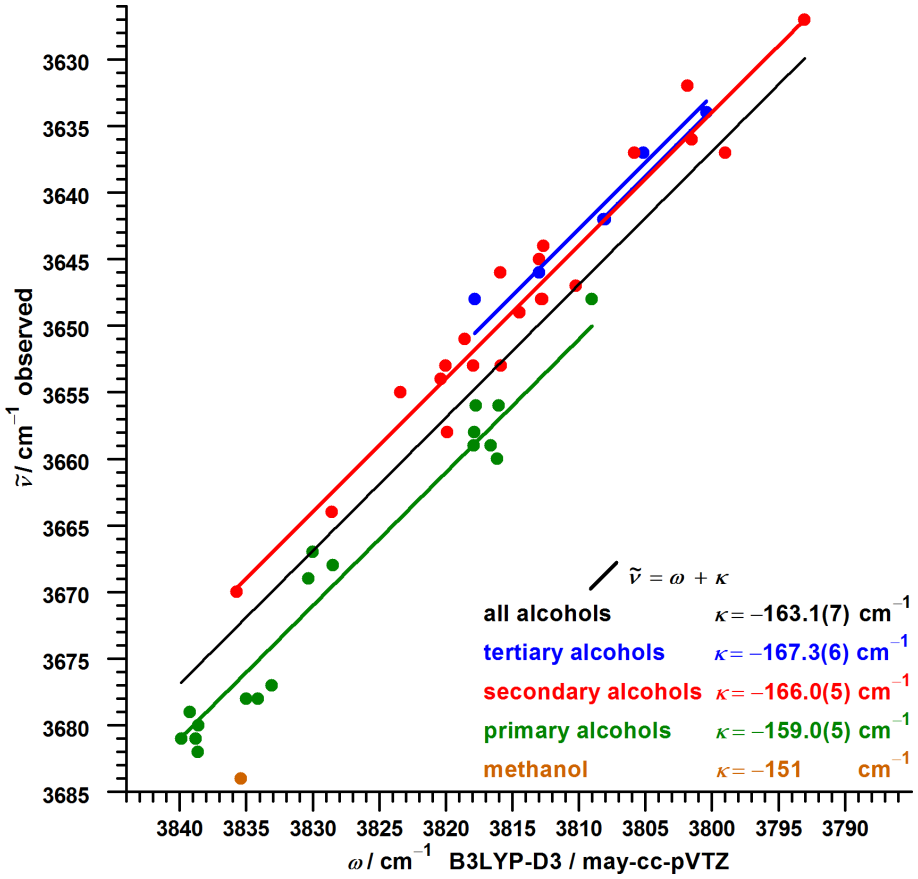

Figure S6: Updated correlation between observed OH stretch fundamental wavenumbers $\tilde{\nu}$ and calculuated harmonic wavenumbers ω for alcohols at B3LYP-D3 level. Linear regressions of the type $\tilde{\nu} = \omega + \kappa$ were performed with a fixed slope of unity and an optimized intercept κ with standard error in parentheses.

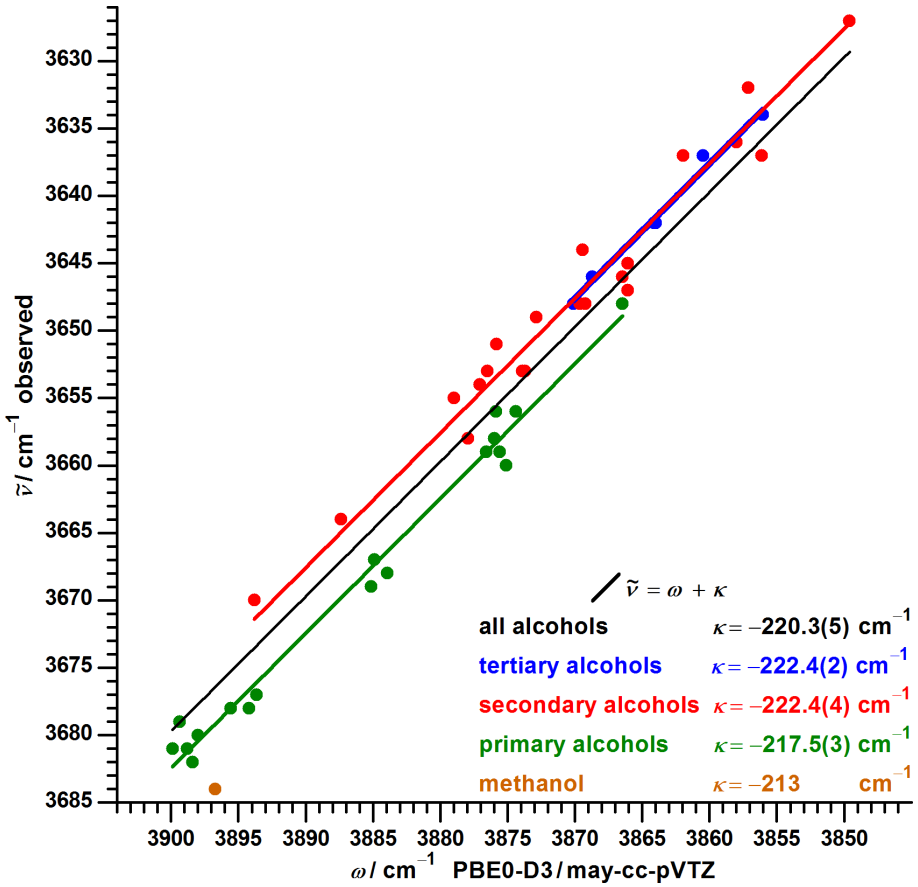

Figure S7: Same as Fig. S6 but for PBE0-D3.

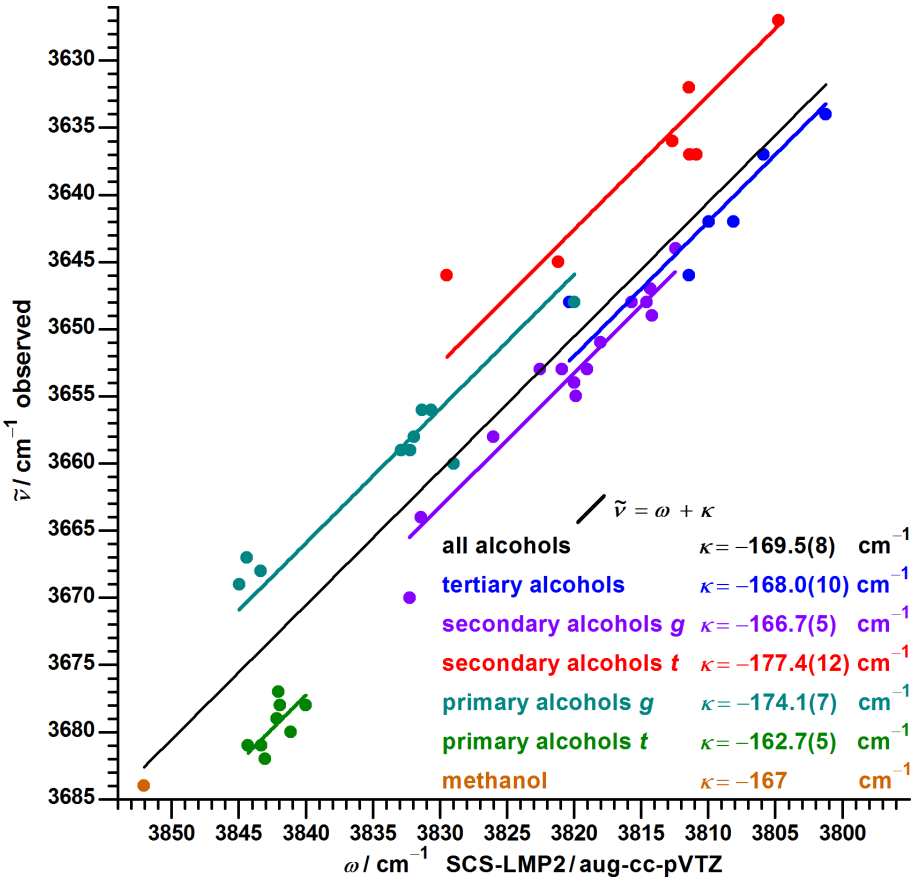

Figure S8: Same as Fig. S6 and S7 but for SCS-LMP2 and separate linear regressions for *gauche* and *trans* conformers of primary and secondary alcohols.

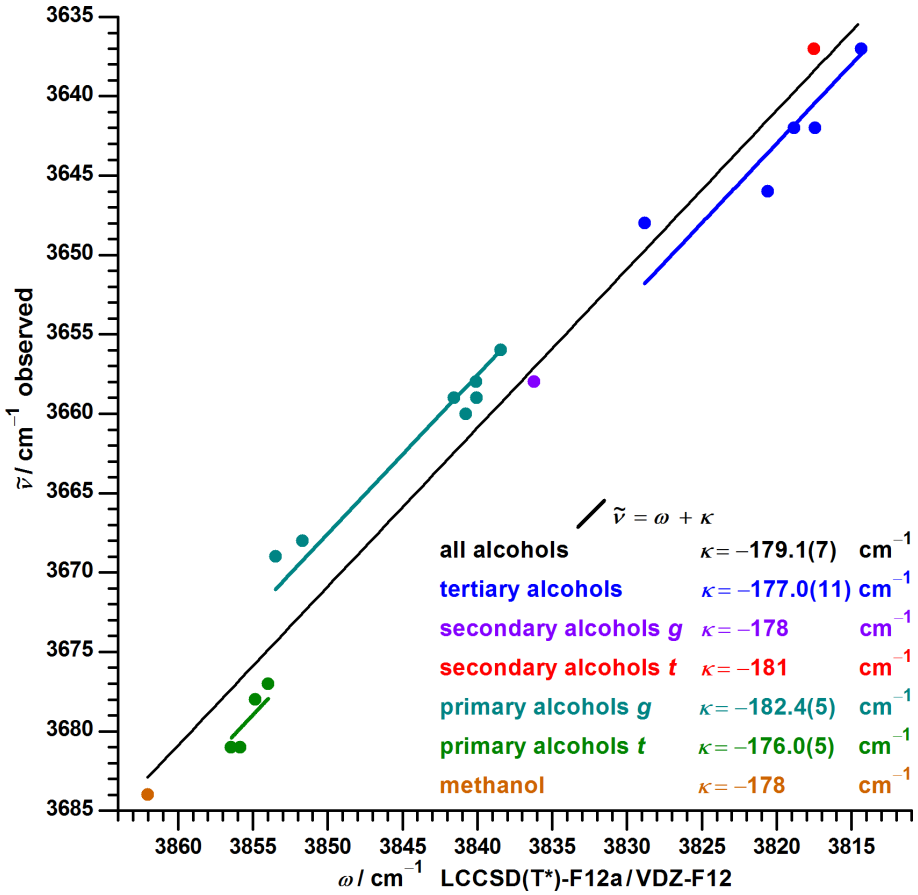

Figure S9: Same as Fig. S8 but for LCCSD(T*) and limited to alcohols with a maximum of five carbon atoms.

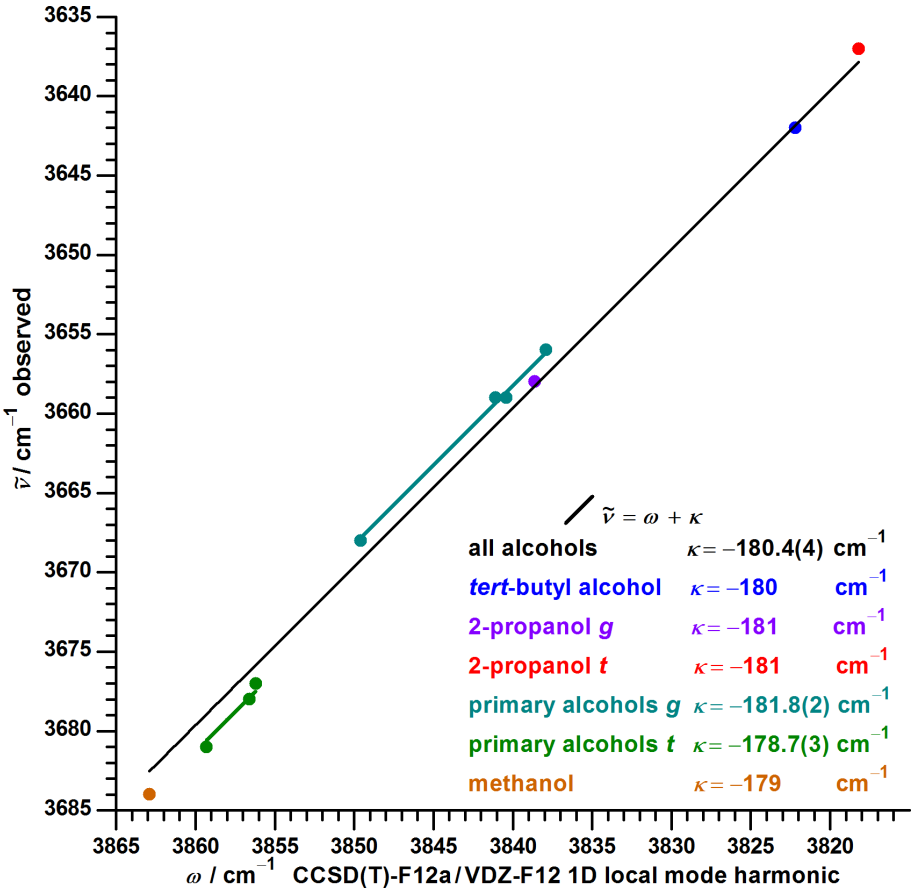

Figure S10: Same as Fig. 9 but for harmonic wavenumbers extracted from reported transitions of the CCSD(T) 1D local mode model in Ref. 12 and limited to the conformers of methanol, ethanol, 1-propanol, 2-propanol and *tert*-butyl alcohol. The figure is unchanged from Fig. 4 of the main document because alcohols of the test set were not investigated with this model.

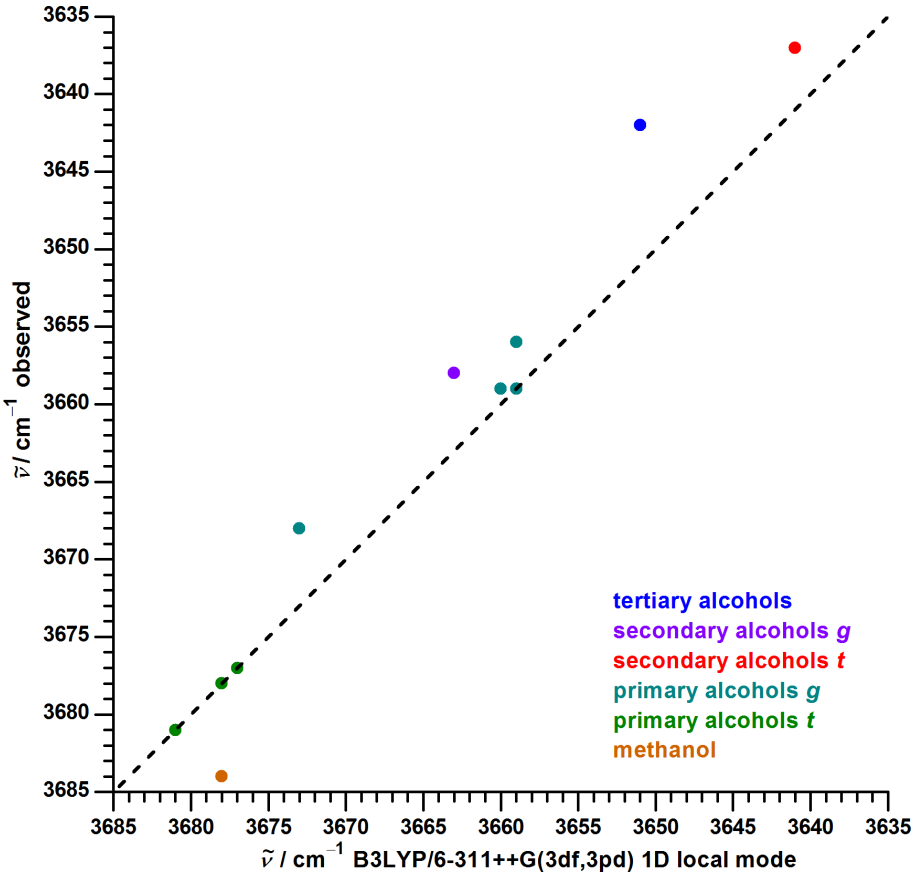

Figure S11: Correlation between observed OH stretch fundamental wavenumbers and anharmonic wavenumbers calculated with the B3LYP 1D local mode model, taken from Ref. 13. The dashed line is not a linear regression but represents perfect agreement between experiment and calculation.

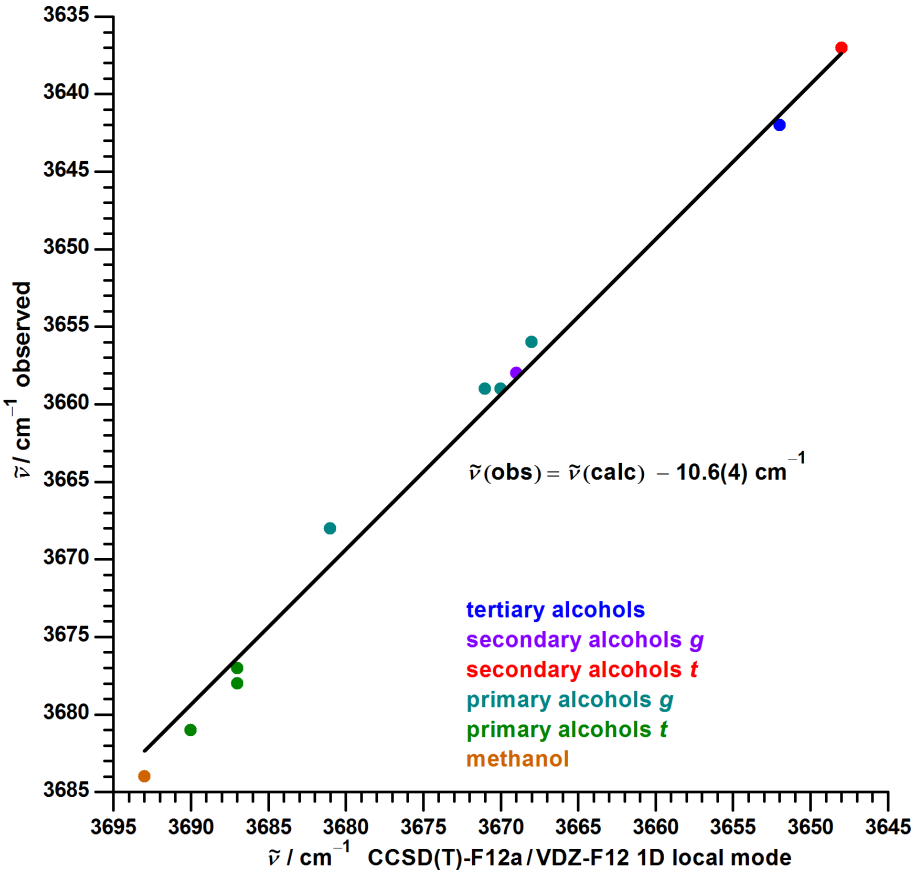

Figure S12: Correlation between observed OH stretch fundamental wavenumbers $\tilde{\nu}$ and fundamental wavenumbers calculated with the CCSD(T) 1D local mode model, taken from Ref. 12. A linear regression $\tilde{\nu}(\text{obs}) = \tilde{\nu}(\text{calc}) + \frac{1}{2}\sum_{j\neq i}^{n} x_{i,j}$ was performed with a fixed slope of unity and an optimized intercept $\frac{1}{2}\sum_{j\neq i}^{n} x_{i,j}$ with standard error in parentheses.

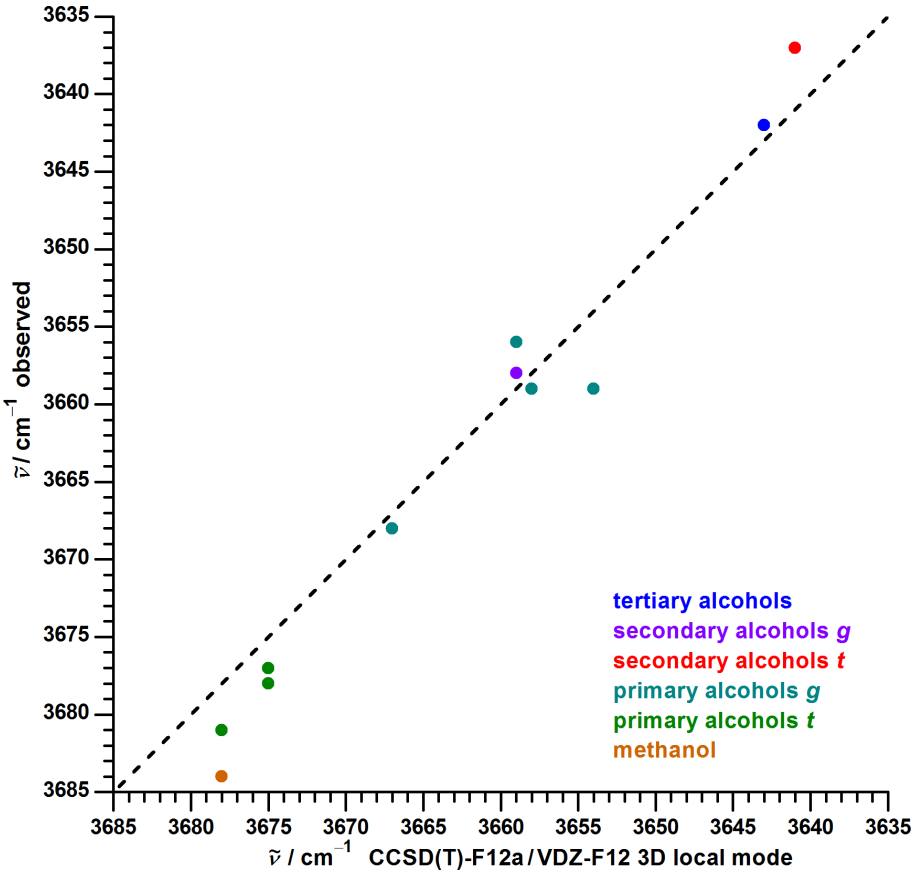

Figure S13: Correlation between observed OH stretch fundamental wavenumbers and calculated anharmonic wavenumbers from the CCSD(T) 3D local mode model, taken from Ref. 12. The dashed line is not a linear regression but represents perfect agreement between experiment and calculation.

4 Two-parameter model for B3LYP-D3 and PBE0-D3

As can be seen in Fig. S6 and S7 for B3LYP-D3 and PBE0-D3 the value of κ is very similar for secondary and tertiary alcohols and changes in roughly equal (but method dependent) steps when moving to primary alcohols and subsequently methanol. One might exploit this regularity to reduce the formal number of parameters to two in the fit without losing much accuracy.

With the two approximate empirical relationships formulated in eqn (1) and (2) one obtains eqn. (3) with $n_{\alpha\mathrm{H}}$ being the number of hydrogen atoms in α position. The function $\max(0,\, n_{\alpha\mathrm{H}}-1)$ yields 0 for tertiary and secondary alcohols, 1 for primary and 2 for methanol.

$$\kappa(\text{primary}) - \kappa(\text{MeOH}) = \kappa(\text{secondary}) - \kappa(\text{primary}) \tag{1}$$

$$\kappa(\text{secondary}) = \kappa(\text{tertiary}) = \kappa(\text{sec./tert.}) \tag{2}$$

$$\tilde{\nu}_i = \omega_i + \kappa(\text{sec./tert.}) + \sigma \cdot \max(0,\, n_{\alpha\mathrm{H}} - 1) \tag{3}$$

This model allows to fit the whole data set with only two adjusted parameters [κ(sec./tert.) and σ] with almost the same accuracy as with independently derived values of κ for each of the four alcohol classes, as it is compared in Table 7 of the main document. However, the assumed interlinkage of parameters is purely empirical.

Table S3: Derived values for the two-parameter approach $\tilde{\nu} = \omega + \kappa(\text{sec./tert.}) + \sigma \cdot \max(0,\, n_{\alpha\mathrm{H}} - 1)$ with standard errors in parentheses for the updated data set

method	κ(sec./tert.) / cm^{-1}	σ / cm^{-1}
B3LYP-D3	−166.3(4)	7.4(6)
PBE0-D3	−222.4(3)	4.9(4)

5 Correlation graphs and corrections for deuterated alcohols

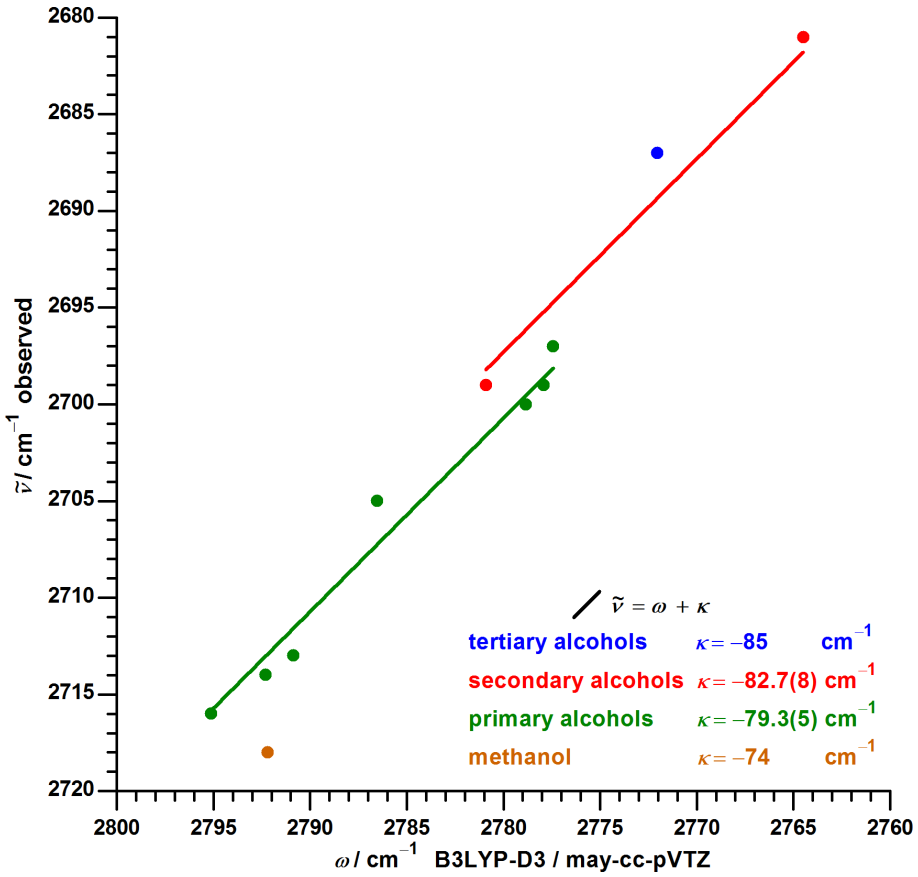

Figure S14: Correlation between observed OD stretch fundamental wavenumbers $\tilde{\nu}$ and calculated harmonic wavenumbers ω for deuterated alcohols at B3LYP-D3 level. Separate for each alcohol class a linear regression $\tilde{\nu} = \omega + \kappa$ was performed with a fixed slope of unity and an optimized intercept κ with standard error in parentheses. Coincidentally, the κ values are rather close to one half of the OH values from Fig. S6.

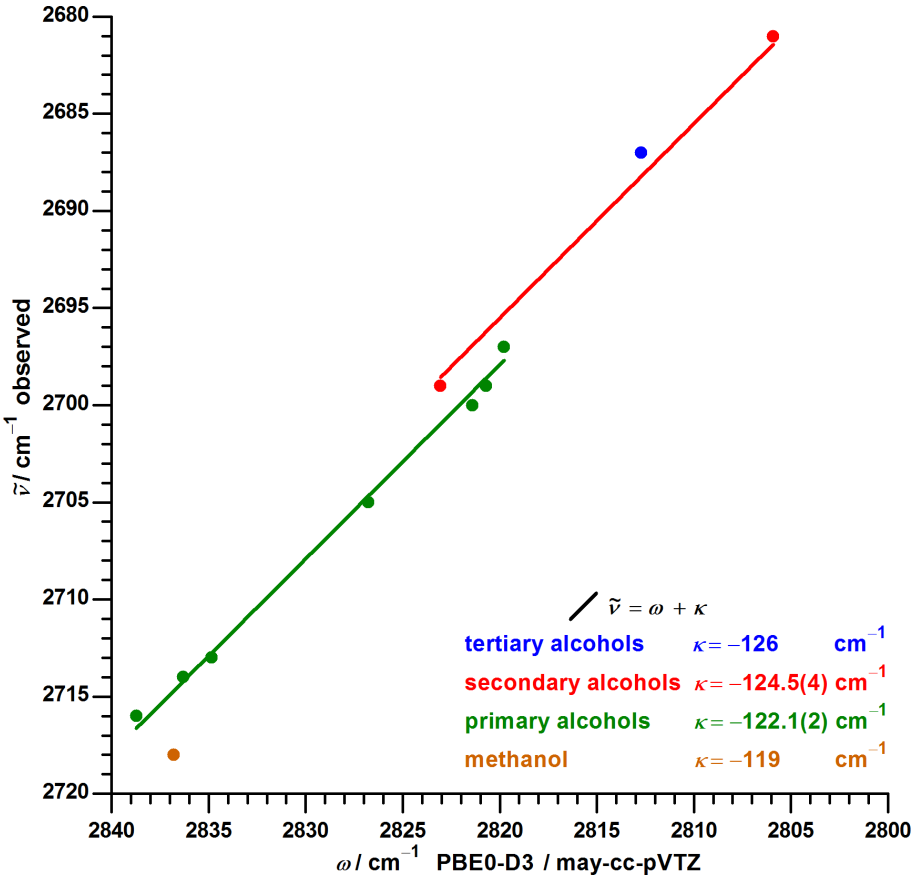

Figure S15: Same as Fig. S14 but for PBE0-D3.

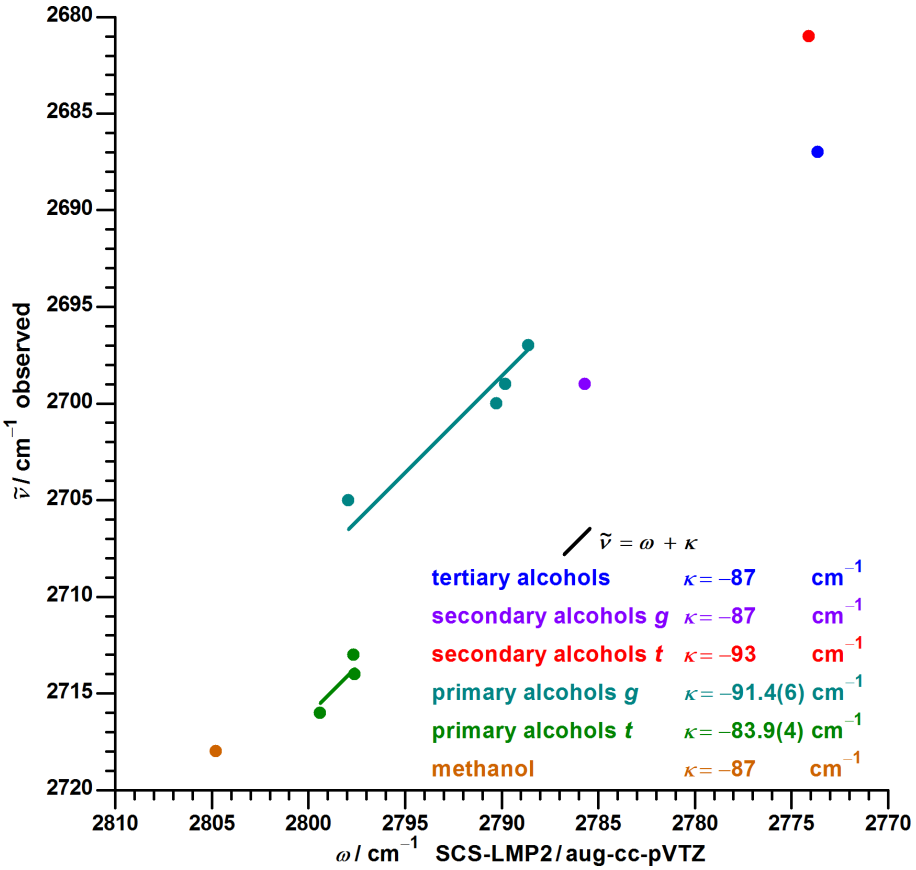

Figure S16: Same as Fig. S14 and S15 but for SCS-LMP2 and separate linear regressions for *gauche* and *trans* conformers of primary and secondary alcohols.

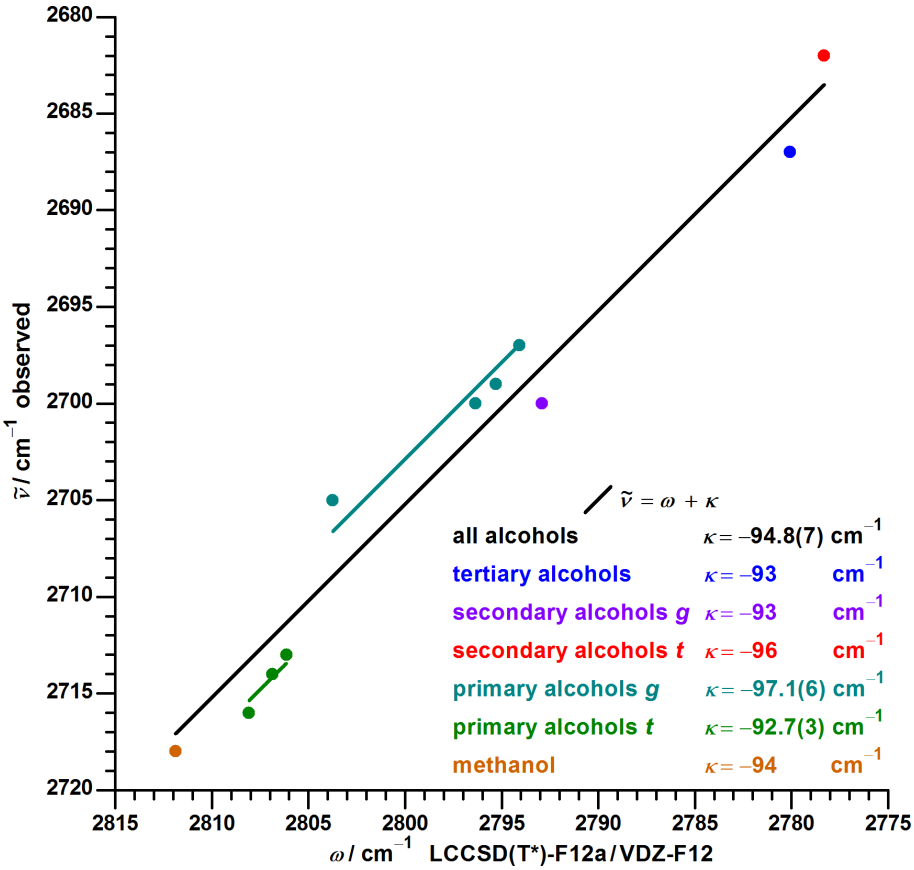

Figure S17: Same as Fig. S16 but for LCCSD(T*).

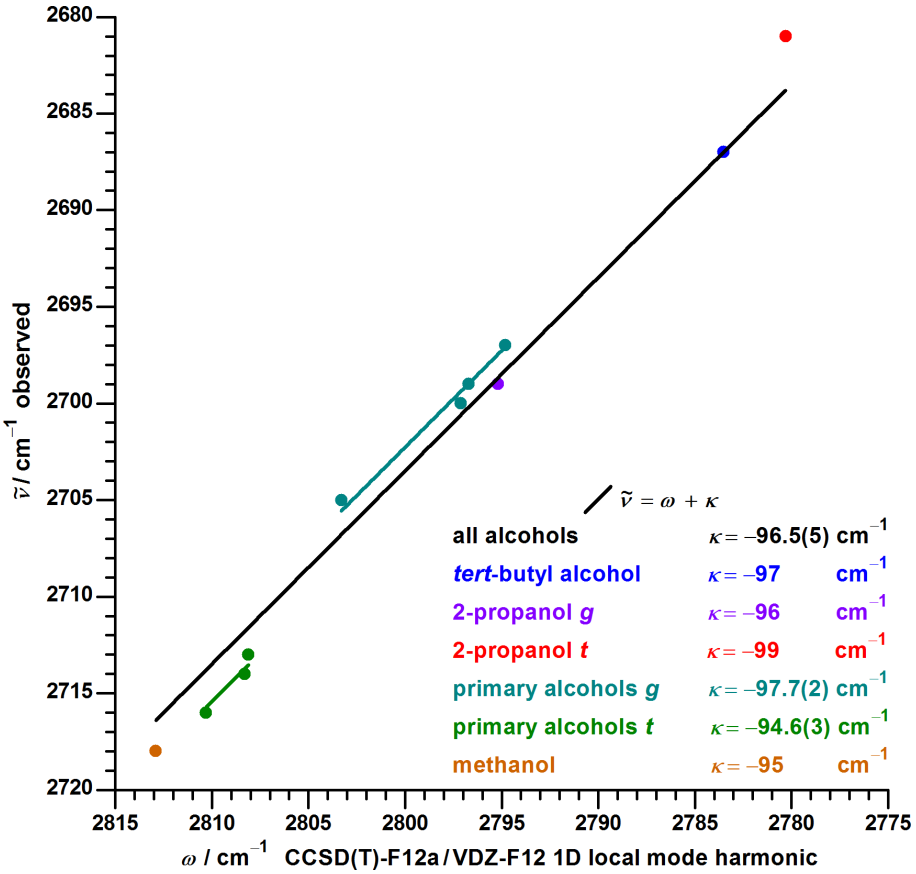

Figure S18: Same as Fig. 16 but for harmonic wavenumbers extracted from reported transitions of the CCSD(T) 1D local mode model in Ref. 12.

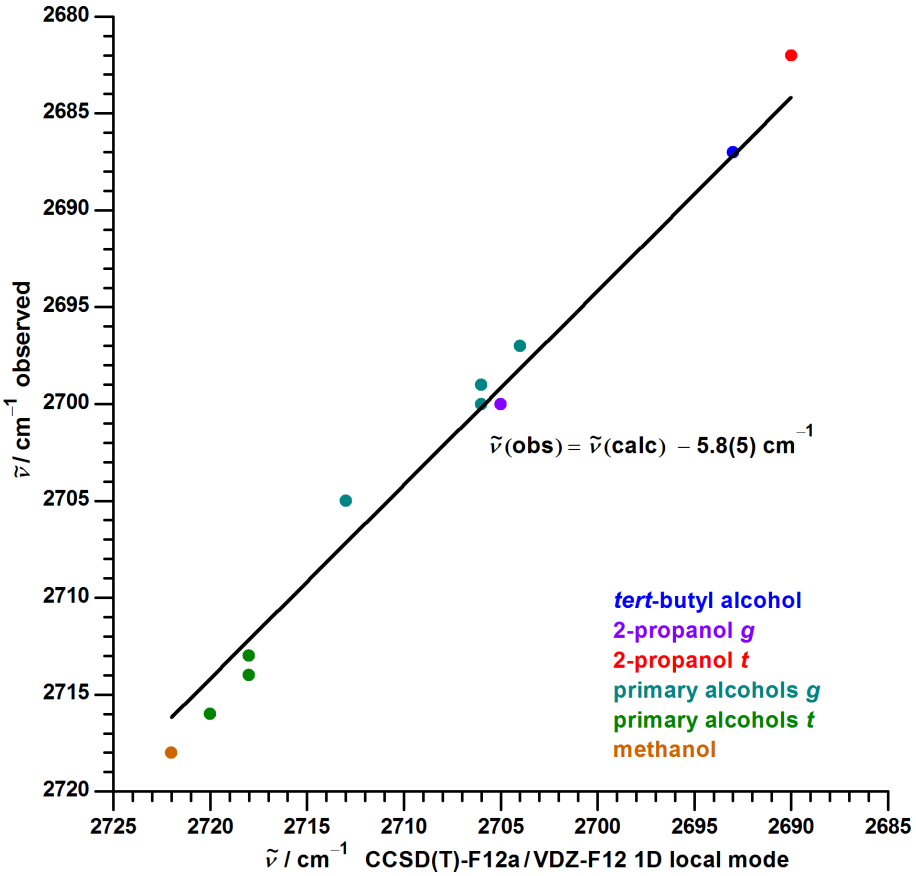

Figure S19: Correlation between observed OD stretch fundamental wavenumbers $\tilde{\nu}$ and calculated fundamental wavenumbers from the CCSD(T) 1D local mode model taken from Ref. 12. A linear regression $\tilde{\nu}(\text{obs}) = \tilde{\nu}(\text{calc}) + \frac{1}{2}\sum_{j\neq i}^{n} x_{i,j}$ was performed with a fixed slope of unity and an optimized intercept $\frac{1}{2}\sum_{j\neq i}^{n} x_{i,j}$ with standard error in parentheses.

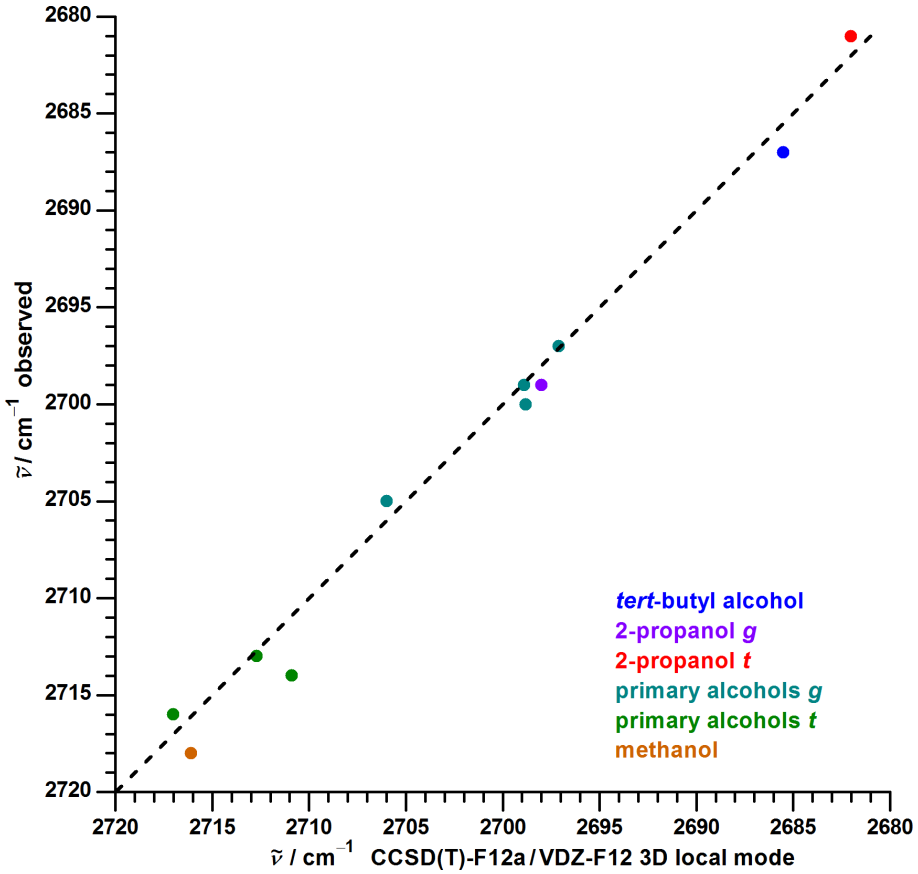

Figure S20: Correlation between observed OD stretch fundamental wavenumbers and calculated anharmonic wavenumbers with the CCSD(T) 3D local mode model, taken from Ref. 12. The diagonal line is not a linear regression but represents perfect agreement between experiment and calculation.

6 Experimental fundamental wavenumbers for alcohol conformers in the data set

Table S4: Experimental fundamental wavenumbers for conformers of primary alcohols used in the model in alphabetic sequence. The respective left most value is used. Values marked with an asterisk* were corrected by $-1\,\mathrm{cm}^{-1}$ to account for the calibration error described in the main document. Values without reference were determined in this work

alcohol	conformer	$\tilde{\nu}_{\mathrm{OH}}$ / cm^{-1}
cyclohexylmethanol	Gg_{het}	3667*[14]
cyclohexylmethanol	Gg_{hom}	3656*[14]
cyclohexylmethanol	Gt	3679*[14]
ethanol	g	3659*[15] 3659.3[16,17] 3667[18]
ethanol	t	3677*[15] 3676.6[16,17] 3682[18]
isopropylmethanol	Gg_{het}	3669*[14]
isopropylmethanol	Gg_{hom}	3658*[14]
isopropylmethanol	Gt	3681*[14]
2-phenylethanol	At	3678[19,20]
phenylmethanol	Gg_{hom}	3648[21] 3648[14] 3649[20] 3650[22]
3-phenyl-1-propanol	AGt	3682[20,23]
3-phenyl-1-propanol	$GG_{\mathrm{hom}}t$	3680[20,23]
1-propanol	Gg_{het}	3668*[24]
1-propanol	Gg_{hom}	3656*[24]
1-propanol	Gt	3681*[24]
1-propanol	Tg	3659*[24]
1-propanol	Tt	3678*[24]
propargyl alcohol	g	3660 (average of split transitions)

Table S5: Same as Table S4 but for secondary alcohols. For 1-indanol, menthol, 2-naphthyl-1-ethanol, neomenthol and 1-phenylethanol the arrangement of the HOCH dihedral is added in parentheses to the literature label

alcohol	conformer	$\tilde{\nu}_{\mathrm{OH}}$ / cm^{-1}
2-adamantol	g	3653 [25]
(−)-borneol	$g-$	3653 3653 [10]
(−)-borneol	$g+$	3670
(−)-borneol	t	3646
cyclohexanol	Eg	3653
cyclohexanol	Et	3636
(*S*)-1-indanol	1eq (t)	3627* [26] 3627 [26] 3627 [26] 3627 [27] 3638 [28]
(*S*)-1-indanol	3eq ($g+$)	3664* [26]
(*S*)-1-indanol	1ax (t)	3637* [26] 3610 [28]
(*S*)-1-indanol	2ax ($g+$)	3651* [26] 3650 [26] 3652 [26] 3654 [27]
(−)-isopinocampheol	$g-$	3644
(−)-isopinocampheol	$g+$	3649 3648 [10]
(−)-isopinocampheol	t	3632
(−)-menthol	*trans* ($g+$)	3654 [29]
(*S*)-2-naphthyl-1-ethanol	Nap$G1$ ($g+$)	3647 [30]
(*S*)-2-naphthyl-1-ethanol	Nap$G2$ ($g+$)	3648 [30]
(+)-neomenthol	*trans* ($g-$)	3654.5 [29]
(−)-1-phenylethanol	$G-g-$ ($g+$)	3648 [21] 3647 [31]
pinacolyl alcohol	t	3645 [10]
2-propanol	g	3558* [32] 3658 [33]
2-propanol	t	3637* [32] 3636 [33]

Table S6: Same as Table S4 but for tertiary alcohols

alcohol	conformer	$\tilde{\nu}_{\mathrm{OH}}$ / cm^{-1}
1-adamantol		3634 [25]
tert-butyl alcohol		3642* [34] 3642 [35]
2-methyl-2-butanol	Gg_{het}	3648*
2-methyl-2-butanol	Gg_{hom}	3637*
2-methyl-2-butanol	Gt	3646*
2-methyl-2-butanol	Tt	3642*

Table S7: Same as Table S4 but for methanol

Alcohol	$\tilde{\nu}_{\mathrm{OH}}$ / cm^{-1}
Methanol	3684 [36] 3684 [17] 3685* [37] 3686 [37] 3683 [38] 3681.5 [39] 3684 [40]

Table S8: Experimental fundamental wavenumbers for conformers of deuterated alcohols used in the model. Values marked with an asterisk* were corrected by $-1\,\mathrm{cm}^{-1}$ to account for the calibration error described in the main document. Values for deuterated 2-propanol are the only ones in the data set not determined in a jet expansion, but from Q-branches at room temperature

alcohol	conformer	$\tilde{\nu}_{\mathrm{OH}}$ / cm^{-1}
methanol		2718*[34]
ethanol	g	2699*[15]
ethanol	t	2713*[15]
1-propanol	Gg_{het}	2705*[24]
1-propanol	Gg_{hom}	2697*[24]
1-propanol	Gt	2716*[24]
1-propanol	Tg	2700*[24]
1-propanol	Tt	2714*[24]
2-propanol	g	2699[12]
2-propanol	t	2681[12]
tert-butyl alcohol		2687*[34]

7 Calculated wavenumbers for alcohol conformers in the data set

Table S9: Calculated harmonic OH stretching wavenumbers in cm^{-1} for methanol

alcohol	conformer	B3LYP-D3	PBE0-D3	SCS-LMP2	LCCSD(T*)	CCSD(T) 1D
methanol		3835.4	3896.7	3852.1	3862.0	3862.9

Table S10: Calculated harmonic OH stretching wavenumbers in cm^{-1} for primary alcohols in the data set of the model

alcohol	conformer	B3LYP-D3	PBE0-D3	SCS-LMP2	LCCSD(T*)	CCSD(T) 1D
cyclohexylmethanol	Gt	3839.2	3899.3	3842.2		
cyclohexylmethanol	Gg_{het}	3830.0	3884.9	3844.4		
cyclohexylmethanol	Gg_{hom}	3817.7	3875.9	3831.3		
ethanol	t	3833.1	3893.6	3842.1	3854.0	3856.2
ethanol	g	3816.6	3875.6	3832.2	3840.1	3840.4
isopropylmethanol	Gg_{het}	3830.3	3885.1	3845.0	3853.5	
isopropylmethanol	Gg_{hom}	3817.9	3876.0	3831.9	3840.1	
isopropylmethanol	Gt	3839.9	3899.9	3843.3	3855.9	
2-phenylethanol	At	3834.1	3894.2	3840.0		
phenylmethanol	Gg_{hom}	3809.0	3866.5	3820.0		
3-phenyl-1-propanol	AGt	3838.6	3898.4	3843.0		
3-phenyl-1-propanol	$GG_{\mathrm{hom}}t$	3838.6	3898.0	3841.1		
1-propanol	Gg_{het}	3828.5	3883.9	3843.4	3851.7	3849.6
1-propanol	Gg_{hom}	3816.0	3874.4	3830.7	3838.4	3837.9
1-propanol	Gt	3838.8	3898.8	3844.3	3856.4	3859.3
1-propanol	Tg	3817.9	3876.6	3832.9	3841.6	3841.1
1-propanol	Tt	3835.0	3895.6	3841.9	3854.8	3856.6
propargyl alcohol	g	3816.2	3883.1	3829.0	3840.8	

Table S11: Calculated harmonic OH stretching wavenumbers in cm^{-1} for secondary alcohols in the data set of the model

alcohol	conformer	B3LYP-D3	PBE0-D3	SCS-LMP2	LCCSD(T*)	CCSD(T) 1D
2-adamantol	g	3817.9	3873.9	3819.0		
(−)-borneol	$g-$	3820.0	3876.5	3822.6		
(−)-borneol	$g+$	3835.7	3893.8	3832.3		
(−)-borneol	t	3815.9	3866.5	3829.5		
cyclohexanol	Eg	3815.9	3873.7	3820.9		
cyclohexanol	Et	3801.5	3858.0	3812.7		
(S)-1-indanol	1eq (t)	3793.0	3849.6	3804.8		
(S)-1-indanol	3eq ($g+$)	3828.6	3887.4	3831.4		
(S)-1-indanol	1ax (t)	3805.8	3861.9	3810.9		
(S)-1-indanol	2ax ($g+$)	3818.6	3875.8	3818.0		
(−)-isopinocampheol	$g-$	3812.7	3869.4	3812.5		
(−)-isopinocampheol	$g+$	3814.5	3872.8	3814.2		
(−)-isopinocampheol	t	3801.8	3857.1	3811.4		
(−)-menthol	*trans* ($g+$)	3820.4	3877.1	3820.0		
(S)-2-naphthyl-1-ethanol	Nap$G1$ ($g+$)	3810.2	3866.0	3814.3		
(S)-2-naphthyl-1-ethanol	Nap$G2$ ($g+$)	3812.8	3869.6	3814.6		
(+)-neomenthol	*trans* ($g-$)	3823.4	3879.0	3819.9		
(−)-1-phenylethanol	$G-g-$ ($g+$)	3812.7	3869.2	3815.7		
pinacolyl alcohol	t	3813.0	3887.0	3821.2		
2-propanol	g	3819.9	3877.9	3826.0	3836.2	3838.6
2-propanol	t	3799.0	3856.1	3811.4	3817.5	3818.2

Table S12: Calculated harmonic OH stretching wavenumbers in cm^{-1} for tertiary alcohols in the data set of the model

alcohol	conformer	B3LYP-D3	PBE0-D3	SCS-LMP2	LCCSD(T*)	CCSD(T) 1D
1-adamantol		3800.4	3856.0	3801.2		
tert-butyl alcohol		3808.0	3864.1	3810.0	3818.9	3822.2
2-methyl-2-butanol	Gg_{het}	3817.8	3870.1	3820.4	3828.8	
2-methyl-2-butanol	Gg_{hom}	3805.2	3860.5	3805.9	3814.3	
2-methyl-2-butanol	Gt	3813.0	3868.7	3811.4	3820.6	
2-methyl-2-butanol	Tt	3808.1	3864.0	3808.1	3817.5	

Table S13: Calculated harmonic OD stretching wavenumbers in cm^{-1} for deuterated alcohols in the data set of the model

alcohol	conformer	B3LYP-D3	PBE0-D3	SCS-LMP2	LCCSD(T*)	CCSD(T) 1D
methanol		2792.2	2836.8	2804.8	2811.9	2812.9
ethanol	t	2790.9	2836.8	2797.7	2806.1	2808.1
ethanol	g	2777.9	2820.7	2789.8	2795.3	2796.7
1-propanol	Gg_{het}	2786.5	2826.8	2797.9	2803.7	2803.3
1-propanol	Gg_{hom}	2777.4	2819.8	2788.6	2794.1	2794.8
1-propanol	Gt	2795.1	2838.7	2799.4	2808.1	2810.3
1-propanol	Tg	2778.8	2821.4	2790.3	2796.4	2797.1
1-propanol	Tt	2792.3	2836.3	2797.6	2806.9	2808.3
2-propanol	g	2780.9	2823.1	2785.7	2792.9	2795.2
2-propanol	t	2764.5	2805.9	2774.1	2778.3	2780.3
tert-butyl alcohol		2772.0	2812.7	2773.6	2780.1	2783.5

Table S14: Calculated fundamental and first overtone OH stretching wavenumbers in cm^{-1} for protiated alcohols from the CCSD(T) 1D and 3D models of Ref. 12 with an additional digit as kindly provided by H. G. Kjaergaard

alcohol	conformer	3D fundamental	1D fundamental	1D first overtone
methanol		3678.1	3692.7	7215.2
ethanol	t	3675.0	3686.8	7204.2
ethanol	g	3654.4	3670.2	7170.2
1-propanol	Gg_{het}	3667.3	3680.6	7192.2
1-propanol	Gg_{hom}	3659.3	3667.6	7164.9
1-propanol	Gt	3678.0	3689.9	7210.4
1-propanol	Tg	3658.3	3670.8	7171.3
1-propanol	Tt	3675.0	3686.9	7204.1
2-propanol	g	3658.7	3668.9	7168.1
2-propanol	t	3640.5	3647.9	7125.5
tert-butyl alcohol		3642.6	3652.3	7134.7

Table S15: Calculated fundamental and first overtone OD stretching wavenumbers in cm^{-1} for deuterated alcohols from the CCSD(T) 1D and 3D models of Ref. 12 with an additional digit as kindly provided by H. G. Kjaergaard

alcohol	conformer	3D fundamental	1D fundamental	1D first overtone
methanol		2716.1	2722.3	5354.0
ethanol	t	2712.7	2717.9	5345.6
ethanol	g	2698.9	2706.0	5321.3
1-propanol	Gg_{het}	2706.0	2713.3	5336.6
1-propanol	Gg_{hom}	2697.1	2704.1	5317.5
1-propanol	Gt	2717.0	2720.1	5350.0
1-propanol	Tg	2698.8	2706.4	5322.1
1-propanol	Tt	2710.9	2718.0	5345.7
2-propanol	g	2698.0	2704.9	5319.5
2-propanol	t	2682.0	2689.7	5288.8
tert-butyl alcohol		2685.5	2692.9	5295.2

8 Importance of the cubic term for describing the OH stretching potential

Truncating the 1D expression of eqn. (1) of the main document after the cubic term results in eqn. (4):

$$G(v) = \omega\left(v+\frac{1}{2}\right) + x\left(v+\frac{1}{2}\right)^2 + y\left(v+\frac{1}{2}\right)^3 \tag{4}$$

The expressions for the fundamental, first and second overtone are given in eqn. (5)–(7):

$$\tilde{\nu}(1 \leftarrow 0) = \omega + 2x + \frac{1}{4}y \tag{5}$$

$$\tilde{\nu}(2 \leftarrow 0) = 2\omega + 6x + \frac{14}{4}y \tag{6}$$

$$\tilde{\nu}(3 \leftarrow 0) = 3\omega + 12x + \frac{123}{4}y \tag{7}$$

From these the constants can be calculated through:

$$\omega = \frac{285}{84}\tilde{\nu}(1 \leftarrow 0) - \frac{117}{84}\tilde{\nu}(2 \leftarrow 0) + \frac{11}{84}\tilde{\nu}(3 \leftarrow 0) \tag{8}$$

$$x = -\frac{17}{14}\tilde{\nu}(1 \leftarrow 0) + \frac{10}{14}\tilde{\nu}(2 \leftarrow 0) - \frac{1}{14}\tilde{\nu}(3 \leftarrow 0) \tag{9}$$

$$y = \frac{3}{21}\tilde{\nu}(1 \leftarrow 0) - \frac{3}{21}\tilde{\nu}(2 \leftarrow 0) + \frac{1}{21}\tilde{\nu}(3 \leftarrow 0) \tag{10}$$

Using the fundamental and first overtone transitions in Table S14 of this document and the second overtone transitions in Tables S2–S9 in the ESI of Ref. 12 one obtains the results in Table S16:

Table S16: Harmonic wavenumbers, diagonal quadratic and cubic anharmonicity constants in cm^{-1} for protiated alcohols extracted from transitions predicted by the CCSD(T) 1D model of Ref. 12. Also given are the differences to the results obtained when the cubic term is truncated in eqn. (4)

alcohol	conformer	ω	$\Delta\omega$	x	Δx	y
methanol		3863.1	0.2	−85.2	−0.2	0.07
ethanol	t	3856.4	0.2	−84.8	−0.3	0.09
ethanol	g	3840.5	0.1	−85.2	−0.1	0.05
1-propanol	Gg_{het}	3849.9	0.3	−84.7	−0.3	0.10
1-propanol	Gg_{hom}	3838.0	0.1	−85.2	−0.2	0.05
1-propanol	Gt	3859.5	0.2	−84.8	−0.2	0.07
1-propanol	Tg	3841.3	0.2	−85.3	−0.2	0.07
1-propanol	Tt	3856.8	0.2	−84.9	−0.2	0.07
2-propanol	g	3838.8	0.2	−84.9	−0.2	0.07
2-propanol	t	3818.5	0.3	−85.3	−0.3	0.10
tert-butyl alcohol		3822.4	0.2	−85.1	−0.3	0.09

9 Additional calculations for the test set

9.1 Propargyl alcohol

Table S17: Calculated relative zero-point-corrected energies, Raman activities and depolarization ratios of the OH-stretching fundamentals for conformers of propargyl alcohol

conformer	method	E^0_{rel}/ kJ mol^{-1}	A_{R}/ Å^{4}u^{-1}	P
g	B3LYP-D3	0		
g	PBE0-D3	0	61	0.17
g	SCS-LMP2	0		
g	LCCSD(T*)	0		
t	B3LYP-D3	6.8		
t	PBE0-D3	7.2	143	0.24
t	SCS-LMP2	5.6		
t	LCCSD(T*)	5.8		

9.2 Cyclohexanol

Table S18: Calculated relative zero-point-corrected energies, relative Gibbs energies at 298 K, Boltzmann population at 298 K, Raman activities and depolarization ratios of the OH-stretching fundamentals for conformers of cyclohexanol

conformer	method	E^0_{rel}/ kJ mol^{-1}	G^{298}_{rel}/ kJ mol^{-1}	p / %	A_{R}/ Å^{4}u^{-1}	P
Eg	B3LYP-D3	0	0	56	123	0.23
Eg	PBE0-D3	0	0	56	115	0.22
Eg	SCS-LMP2	0	0	58		
Et	B3LYP-D3	0.3	0.2	25	67	0.18
Et	PBE0-D3	0.3	0.2	26	65	0.17
Et	SCS-LMP2	1.0	0.9	20		
Ag	B3LYP-D3	3.1	3.2	15	100	0.23
Ag	PBE0-D3	3.4	3.6	13	94	0.22
Ag	SCS-LMP2	2.6	2.8	19		
At	B3LYP-D3	4.9	4.8	4	39	0.11
At	PBE0-D3	5.0	4.9	4	37	0.11
At	SCS-LMP2	6.1	6.1	2		

9.3 (−)-Borneol

Table S19: Calculated relative zero-point-corrected energies, Raman activities and depolarization ratios of the OH-stretching fundamentals for conformers of (−)-borneol

conformer	method	E^0_{rel}/ kJ mol^{-1}	A_{R}/ Å^4 u^{-1}	P
$g-$	B3LYP-D3	0		
$g-$	PBE0-D3	0	86	0.21
$g-$	SCS-LMP2	0		
$g+$	B3LYP-D3	0.9		
$g+$	PBE0-D3	1.0	129	0.24
$g+$	SCS-LMP2	0.1		
t	B3LYP-D3	1.7		
t	PBE0-D3	1.5	45	0.13
t	SCS-LMP2	2.9		

9.4 (−)-Isopinocampheol

Table S20: Calculated relative zero-point-corrected energies, Raman activities and depolarization ratios of the OH-stretching fundamentals for conformers of (−)-isopinocampheol

conformer	method	E^0_{rel}/ kJ mol^{-1}	A_{R}/ Å^4 u^{-1}	P
$g-$	B3LYP-D3	0.4		
$g-$	PBE0-D3	0.4	98	0.22
$g-$	SCS-LMP2	0.8		
$g+$	B3LYP-D3	0		
$g+$	PBE0-D3	0	127	0.24
$g+$	SCS-LMP2	0		
t	B3LYP-D3	1.0		
t	PBE0-D3	0.9	61	0.17
t	SCS-LMP2	2.1		

9.5 2-Methyl-2-butanol

Table S21: Calculated relative zero-point-corrected energies, relative Gibbs energies at 298 K, Raman activities and depolarization ratios of the OH-stretching fundamentals for conformers of 2-methyl-2-butanol

conformer	method	E^0_{rel}/ kJ mol^{-1}	G^{298}_{rel}/ kJ mol^{-1}	A_{R}/ Å^4 u^{-1}	P
Gg_{het}	B3LYP-D3	0.4	0.2	72	0.18
Gg_{het}	PBE0-D3	0.3	0.1	68	0.17
Gg_{het}	SCS-LMP2	0.7			
Gg_{het}	LCCSD(T*)	0.7	0.3		
Gt	B3LYP-D3	0.2	0.0	95	0.21
Gt	PBE0-D3	0.1	0.0	91	0.21
Gt	SCS-LMP2	−0.1			
Gt	LCCSD(T*)	0.03	−0.3		
Tt	B3LYP-D3	0.7	0.4	107	0.22
Tt	PBE0-D3	0.9	0.6	101	0.21
Tt	SCS-LMP2	1.1			
Tt	LCCSD(T*)	1.1	0.5		
Gg_{hom}	B3LYP-D3	0	0	86	0.20
Gg_{hom}	PBE0-D3	0	0	82	0.20
Gg_{hom}	SCS-LMP2	0	0		
Gg_{hom}	LCCSD(T*)	0	0		
Tg	B3LYP-D3	0.5	0.2	89	0.20
Tg	PBE0-D3	0.7	0.3	85	0.20
Tg	SCS-LMP2	0.9			
Tg	LCCSD(T*)	0.9	0.3		

10 Tests for hydrogen-bonded conformers

The performance of the model is tested in Tables S22–S27 for a selection of hydrogen-bonded alcohols reported in the literature with π, N, O, F and Cl acceptors. The predictions with PBE0-D3 underestimate in almost all cases the transition wavenumber, which is equivalent to an overestimation of the downshift. Well predicted by B3LYP-D3 and SCS-LMP2 are the wavenumbers of the OH$\cdots\pi$ hydrogen bonded conformers of 2-phenylethanol [19,20] and 3-phenyl-1-propanol. [20,23] This is in line with findings for the most elementary intermolecular example methanol+ethylene, for which it was concluded that changes in diagonal and off-diagonal anharmonicity upon hydrogen bond formation mostly cancel each other, therefore harmonic predictions by SCS-LMP2 and LCCSD(T*) were found to give a good estimate of the downshift. [41] The fundamental wavenumbers for alcohols with weak OH$\cdots$F hydrogen bonds tend to be underestimated by all methods, which can at least partly be attributed to a lowered diagonal anharmonicity [13,42,43] compared to non-hydrogen-bonded alcohols. [16] Spectral positions for alcohols with OH$\cdots$Cl hydrogen bonds [44] are instead overestimated by all methods but PBE0-D3, when applying the corresponding model. For N and O acceptors, as in aminoethanols [45] respectively glycols [46] and alpha-hydroxy carbonyl compounds, [47–49] SCS-LMP2 and LCCSD(T*) model predictions increasingly overestimate transitions wavenumbers with the strength of the hydrogen bond, judged by the spectral position. This might be in part explained with an increase of diagonal anharmonicity as found for intermolecular OH$\cdots$O hydrogen bonds. [16] However, for the methanol dimer it was concluded that this is actually outweighed by a decrease of the off-diagonal contributions. [50] B3YLP-D3 predictions are overall closer to experiment for these acceptor types and show a mix of over- and underestimations. Fundamental OH stretching wavenumbers of hydroxy groups in glycols which do not donate but accept a hydrogen bond are well predicted by all tested methods within $2\,\mathrm{cm}^{-1}$.

Table S22: Assignments, experimental band positions and deviations of the model predictions for the OH-stretching fundamental of alcohol conformers with intramolecular OH$\cdots\pi$ hydrogen bonds. The updated values for κ from Fig. S6–S9 are used

alcohol	conformer	method	$\tilde{\nu}/\,\mathrm{cm}^{-1}$	$(\omega+\kappa-\tilde{\nu}_{\mathrm{exp}})/\,\mathrm{cm}^{-1}$
2-phenylethanol	*Gg*-π	experiment	3626 [19]	
		B3LYP-D3	3630	4
		PBE0-D3	3619	−7
		SCS-LMP2	3624	−2
3-phenyl-1-propanol	*GG′g*-π	experiment	3630 [20,23]	
		B3LYP-D3	3633	3
		PBE0-D3	3616	−14
		SCS-LMP2	3628	−2

Table S23: Same as Table S22 but for intramolecular OH$\cdots$N hydrogen bonds

alcohol	conformer	method	$\tilde{\nu}/\,\mathrm{cm}^{-1}$	$(\omega+\kappa-\tilde{\nu}_{\mathrm{exp}})/\,\mathrm{cm}^{-1}$
aminoethanol	$g'Gg'$	experiment	3569[45]	
		B3LYP-D3	3568	−1
		PBE0-D3	3541	−28
		SCS-LMP2	3586	17
		LCCSD(T*)	3585	16
N-methylaminoethanol	*t*-$g'Gg'$	experiment	3569[45]	
		B3LYP-D3	3571	2
		PBE0-D3	3547	−22
		SCS-LMP2	3587	18
		LCCSD(T*)	3589	20
N-methylaminoethanol	*g*-$g'Gg'$	experiment	3543[45]	
		B3LYP-D3	3550	7
		PBE0-D3	3520	−23
		SCS-LMP2	3571	28
		LCCSD(T*)	3568	25
N, *N*-dimethylaminoethanol	$g'Gg'$	experiment	3542[45]	
		B3LYP-D3	3551	9
		PBE0-D3	3525	−17
		SCS-LMP2	3570	28
		LCCSD(T*)		

Table S24: Same as Table S22 but for intramolecular OH$\cdots$O hydrogen bonds

alcohol	conformer	method	$\tilde{\nu}/\,\mathrm{cm}^{-1}$	$(\omega+\kappa-\tilde{\nu}_{\mathrm{exp}})/\,\mathrm{cm}^{-1}$
2-methoxyethanol	$gG'T$	experiment	3635 [51]	
		B3LYP-D3	3641	6
		PBE0-D3	3635	0
		SCS-LMP2	3640	5
		LCCSD(T*)		
ethylene glycol	M acceptor	experiment	3689 [46]	
		B3LYP-D3	3687	−2
		PBE0-D3	3688	−1
		SCS-LMP2	3690	1
		LCCSD(T*)	3689	0
ethylene glycol	M donor	experiment	3636 [46]	
		B3LYP-D3	3639	3
		PBE0-D3	3632	−4
		SCS-LMP2	3641	5
		LCCSD(T*)	3640	4
ethylene glycol	M' acceptor	experiment	3656 [46]	
		B3LYP-D3	3655	−1
		PBE0-D3	3654	−2
		SCS-LMP2	3655	−1
		LCCSD(T*)	3655	−1
ethylene glycol	M' donor	experiment	3623 [46]	
		B3LYP-D3	3623	0
		PBE0-D3	3614	−9
		SCS-LMP2	3629	6
		LCCSD(T*)	3627	4
trans-1,2-cyclohexanediol	M acceptor	experiment	3667 [46]	
		B3LYP-D3	3665	−2
		PBE0-D3	3666	−1
		SCS-LMP2	3667	0
		LCCSD(T*)		
trans-1,2-cyclohexanediol	M donor	experiment	3628 [46]	
		B3LYP-D3	3628	0
		PBE0-D3	3621	−7
		SCS-LMP2	3636	8
		LCCSD(T*)		
trans-1,2-cyclohexanediol	M' acceptor	experiment	3628 [46]	
		B3LYP-D3	3629	−1
		PBE0-D3	3628	0
		SCS-LMP2	3629	1
		LCCSD(T*)		
trans-1,2-cyclohexanediol	M' donor	experiment	3616 [46]	
		B3LYP-D3	3612	−4
		PBE0-D3	3604	−12
		SCS-LMP2	3625	9
		LCCSD(T*)		

Table S25: Continuation of Table S24. In the listed alpha-hydroxy carbonyl compounds the HOCC dihedral adopts an eclipsed arrangement not present in the training set. For the wavefunction-based methods the correction for *gauche* conformers is used

alcohol	conformer	method	$\tilde{\nu}/\,\mathrm{cm}^{-1}$	$(\omega+\kappa-\tilde{\nu}_{\mathrm{exp}})/\,\mathrm{cm}^{-1}$
glycolic acid	SSC	experiment	3578[49]	
		B3LYP-D3	3569	−9
		PBE0-D3	3547	−31
		SCS-LMP2	3595	17
		LCCSD(T*)		
glycolaldehyde	M4	experiment	3549[48]	
		B3LYP-D3	3549	−3
		PBE0-D3	3522	−27
		SCS-LMP2	3574	25
		LCCSD(T*)	3556	7
hydroxy acetone	Cc	experiment	3525[47]	
		B3LYP-D3	3518	−7
		PBE0-D3	3489	−36
		SCS-LMP2	3556	31
		LCCSD(T*)		

Table S26: Same as Table S22 but for intramolecular OH$\cdots$F hydrogen bonds

alcohol	conformer	method	$\tilde{\nu}/\,\mathrm{cm}^{-1}$	$(\omega+\kappa-\tilde{\nu}_{\mathrm{exp}})/\,\mathrm{cm}^{-1}$
2-fluoroethanol	Gg_{het}	experiment	3652[44]	
		B3LYP-D3	3652	0
		PBE0-D3	3650	−2
		SCS-LMP2	3651	−1
		LCCSD(T*)	3650	−2
2,2-difluoroethanol	Gg_{hom}	experiment	3656[44]	
		B3LYP-D3	3654	−2
		PBE0-D3	3652	−4
		SCS-LMP2	3654	−2
		LCCSD(T*)		
2,2,2-trifluoroethanol	g	experiment	3657[44]	
		B3LYP-D3	3654	−3
		PBE0-D3	3652	−5
		SCS-LMP2	3655	−2
		LCCSD(T*)		
3,3,3-trifluoropropanol	Gg_{het}	experiment	3668[52]	
		B3LYP-D3	3664	−4
		PBE0-D3	3661	−7
		SCS-LMP2	3667	−1
		LCCSD(T*)		
1,1,1,3,3,3-hexafluoro-2-propanol	g	experiment	3667[53]	
		B3LYP-D3	3656	−11
		PBE0-D3	3653	−14
		SCS-LMP2	3667	0
		LCCSD(T*)		
1,1,1,3,3,3-hexafluoro-2-propanol	t	experiment	3623[53]	
		B3LYP-D3	3618	−5
		PBE0-D3	3614	−9
		SCS-LMP2	3622	−1
		LCCSD(T*)		

Table S27: Same as Table S22 but for intramolecular OH$\cdots$Cl hydrogen bonds

alcohol	conformer	method	$\tilde{\nu}/\,\mathrm{cm}^{-1}$	$(\omega+\kappa-\tilde{\nu}_{\mathrm{exp}})/\,\mathrm{cm}^{-1}$
2-chloroethanol	Gg_{het}	experiment	3626 [44]	
		B3LYP-D3	3630	4
		PBE0-D3	3620	−6
		SCS-LMP2	3635	9
		LCCSD(T*)	3631	5
2,2-dichloroethanol	Gg_{hom}	experiment	3629 [44]	
		B3LYP-D3	3633	4
		PBE0-D3	3624	−5
		SCS-LMP2	3639	10
		LCCSD(T*)		
2,2,2-trichloroethanol	g	experiment	3628 [44]	
		B3LYP-D3	3633	5
		PBE0-D3	3623	−5
		SCS-LMP2	3638	10
		LCCSD(T*)		

11 Sample inputs

Before calculating other alcohols it is recommended to do a quick test with methanol to check whether the expected result in the included comment is reproduced. Default settings might change in future versions of the software, so that adjustments to the input might become necessary. Note that the provided cartesian coordinates are typically not the final optimized values.

For the SCS-LMP2 and LCCSD(T*) calculations of protiated alcohols the Molpro default averaged masses for the isotopes in natural abundance were used. Test calculations indicate that using the masses of the main isotopes (as for the deuterated alcohols and DFT calculations) increases OH stretching wavenumbers uniformly by about $0.2\,\mathrm{cm}^{-1}$.

The LCCSD(T*) input closely follows the one used in Ref. 36, where more information on the manual triple scaling procedure can be found.

11.1 B3LYP-D3 protiated alcohols

```
%nprocshared=12
%mem=24GB
# B3LYP empiricaldispersion=GD3BJ may-cc-pVTZ int=ultrafine fopt=verytight freq

sample input for Gaussian and protiated methanol at B3LYP-D3 level
omega(OH)=3835.4 cm-1  HF=-115.7791605
mind to add two blank lines at the end of the input

0 1
 C                  0.66700800   -0.02037000    0.00000000
 H                  1.08330700    0.98481800   -0.00000400
 H                  1.02680100   -0.54422200   -0.89076900
 H                  1.02680200   -0.54421600    0.89077300
 O                 -0.74862300    0.12207900    0.00000000
 H                 -1.14998000   -0.75079500    0.00000000
```

11.2 B3LYP-D3 deuterated alcohols

```
%nprocshared=12
%mem=24GB
# B3LYP empiricaldispersion=GD3BJ may-cc-pVTZ int=ultrafine fopt=verytight freq

sample input for Gaussian and deuterated methanol at B3LYP-D3 level
omega(OD)=2792.2 cm-1  HF=-115.7791605
mind to add two blank lines at the end of the input

0 1
 C                         0.66700800   -0.02037000    0.00000000
 H                         1.08330700    0.98481800   -0.00000400
 H                         1.02680100   -0.54422200   -0.89076900
 H                         1.02680200   -0.54421600    0.89077300
 O                        -0.74862300    0.12207900    0.00000000
 H(Iso=2)                 -1.14998000   -0.75079500    0.00000000
```

11.3 PBE0-D3 protiated alcohols

```
%nprocshared=12
%mem=24GB
# PBE1PBE empiricaldispersion=GD3BJ may-cc-pvtz int=ultrafine fopt=verytight freq

sample input for Gaussian and protiated methanol at PBE0-D3 level
omega(OH)=3896.7 cm-1  HF=-115.638438 H
mind to add two blank lines at the end of the input

0 1
 C                  0.66700800   -0.02037000    0.00000000
 H                  1.08330700    0.98481800   -0.00000400
 H                  1.02680100   -0.54422200   -0.89076900
 H                  1.02680200   -0.54421600    0.89077300
 O                 -0.74862300    0.12207900    0.00000000
 H                 -1.14998000   -0.75079500    0.00000000
```

11.4 PBE0-D3 deuterated alcohols

```
%nprocshared=12
%mem=24GB
# PBE1PBE empiricaldispersion=GD3BJ may-cc-pvtz int=ultrafine fopt=verytight freq

sample input for Gaussian and deuterated methanol at PBE0-D3 level
omega(OD)=2836.8 cm-1  HF=-115.638438 H
mind to add two blank lines at the end of the input

0 1
 C                         0.66700800   -0.02037000    0.00000000
 H                         1.08330700    0.98481800   -0.00000400
 H                         1.02680100   -0.54422200   -0.89076900
 H                         1.02680200   -0.54421600    0.89077300
 O                        -0.74862300    0.12207900    0.00000000
 H(Iso=2)                 -1.14998000   -0.75079500    0.00000000
```

11.5 SCS-LMP2 protiated alcohols

```
! sample input for Molpro and protiated methanol at SCS-LMP2 level
! omega(OH)=3852.1 cm-1  E_SCSMP2 = -115.52532387 H
memory,450,m
nosym
basis=aug-cc-pVTZ
set,geomtyp=xyz
geometry={
 C                  0.66700800   -0.02037000    0.00000000
 H                  1.08330700    0.98481800   -0.00000400
 H                  1.02680100   -0.54422200   -0.89076900
 H                  1.02680200   -0.54421600    0.89077300
 O                 -0.74862300    0.12207900    0.00000000
 H                 -1.14998000   -0.75079500    0.00000000
}

optg,gaussian,gradient=1.5E-5,grms=1E-5,step=6E-5,srms=4E-5,energy=1E-8,procedure=runmp2
runmp2={df-hf;accu,16;df-lmp2,scsgrd=1,npasel=0.03,cpldel=2}
frequencies,symm=no
e_mp2=emp2
e_scsmp2=emp2_scs
e_final=energy
```

11.6 SCS-LMP2 deuterated alcohols

```
! sample input for Molpro and deuterated methanol at SCS-LMP2 level
! omega(OD)=2804.8 cm-1  E_SCSMP2 = -115.52532387 H
memory,450,m
nosym
basis=aug-cc-pVTZ
mass,H1=1.00782503223,H2=2.01410177812,C=12,O=15.99491461957
set,geomtyp=xyz
geometry={
 C                  0.66700800   -0.02037000    0.00000000
 H1                 1.08330700    0.98481800   -0.00000400
 H1                 1.02680100   -0.54422200   -0.89076900
 H1                 1.02680200   -0.54421600    0.89077300
 O                 -0.74862300    0.12207900    0.00000000
 H2                -1.14998000   -0.75079500    0.00000000
}

optg,gaussian,gradient=1.5E-5,grms=1E-5,step=6E-5,srms=4E-5,energy=1E-8,procedure=runmp2
runmp2={df-hf;accu,16;df-lmp2,scsgrd=1,npasel=0.03,cpldel=2}
frequencies,symm=no
e_mp2=emp2
e_scsmp2=emp2_scs
e_final=energy
```

11.7 LCCSD(T*) protiated alcohols

```
! sample input for Molpro and methanol at LCCSD(T*) level
! omega(OH)=3862.0 cm-1
! DF-LCCSD(T)-F12A/cc-pVDZ-F12 energy=-115.6014625477 H
memory,900,m

gthresh,energy=1e-10,zero=1e-16

basis,cc-pvdz-f12

Orient,mass
symmetry,nosym
angstrom
geometry={
 C          0.0130132744        0.0000000026       -0.7286984177
 O         -0.0639775906       -0.0000000056        0.6905989492
 H          0.5202856850       -0.8902803311       -1.1086909953
 H          0.5202783321        0.8902843772       -1.1086913098
 H         -1.0097972059       -0.0000042098       -1.0975017125
 H          0.8297016934        0.0000002216        1.0362045991
}
{df-hf
accu,16}

{df-lccsd(t)-f12a
local,loc_method=pipek,npasel=0.03
pipek,delete=2}

E_CCSDF12A = _ENERGC(1) !LCCSD-F12A "base" energy
E_TRIPF12A = _ENERGY(1) - E_CCSDF12A !(T0) triples contribution, unscaled
E_MP2CORR = _EMP2_SING + _EMP2_TRIP !LMP2 correlation energy
E_MP2F12CORR = E_MP2CORR + _EF12 !LMP2-F12 correlation energy
E_CHECK = E_CCSDF12A + E_TRIPF12A !For checking against LCCSD(T0)-F12A results
E_TARGET = E_CCSDF12A + E_TRIPF12A * E_MP2F12CORR / E_MP2CORR  !"Target" energy

{optg,gaussian,gradient=1.5E-5,grms=1E-5,step=6E-5,srms=4E-5,energy=1E-8
step,0.1,0.1,0.1
variable,E_TARGET}

{frequencies
variable,E_TARGET}
```

11.8 LCCSD(T*) deuterated alcohols

```
! sample input for Molpro and deuterated methanol at LCCSD(T*) level
! omega(OD)=2811.9 cm-1
! DF-LCCSD(T)-F12A/cc-pVDZ-F12 energy=-115.6014625477 H
memory,900,m

gthresh,energy=1e-10,zero=1e-16

basis,cc-pvdz-f12

mass,H1=1.00782503223,H2=2.01410177812,C=12,O=15.99491461957
Orient,mass
symmetry,nosym
angstrom
geometry={
 C          0.0130132744        0.0000000026       -0.7286984177
 O         -0.0639775906       -0.0000000056        0.6905989492
 H1         0.5202856850       -0.8902803311       -1.1086909953
 H1         0.5202783321        0.8902843772       -1.1086913098
 H1        -1.0097972059       -0.0000042098       -1.0975017125
 H2         0.8297016934        0.0000002216        1.0362045991
}
{df-hf
accu,16}

{df-lccsd(t)-f12a
local,loc_method=pipek,npasel=0.03
pipek,delete=2}

E_CCSDF12A = _ENERGC(1) !LCCSD-F12A "base" energy
E_TRIPF12A = _ENERGY(1) - E_CCSDF12A !(T0) triples contribution, unscaled
E_MP2CORR = _EMP2_SING + _EMP2_TRIP !LMP2 correlation energy
E_MP2F12CORR = E_MP2CORR + _EF12 !LMP2-F12 correlation energy
E_CHECK = E_CCSDF12A + E_TRIPF12A !For checking against LCCSD(T0)-F12A results
E_TARGET = E_CCSDF12A + E_TRIPF12A * E_MP2F12CORR / E_MP2CORR  !"Target" energy

{optg,gaussian,gradient=1.5E-5,grms=1E-5,step=6E-5,srms=4E-5,energy=1E-8
step,0.1,0.1,0.1
variable,E_TARGET}

{frequencies
variable,E_TARGET}
```

12 Extended range spectra for the test set

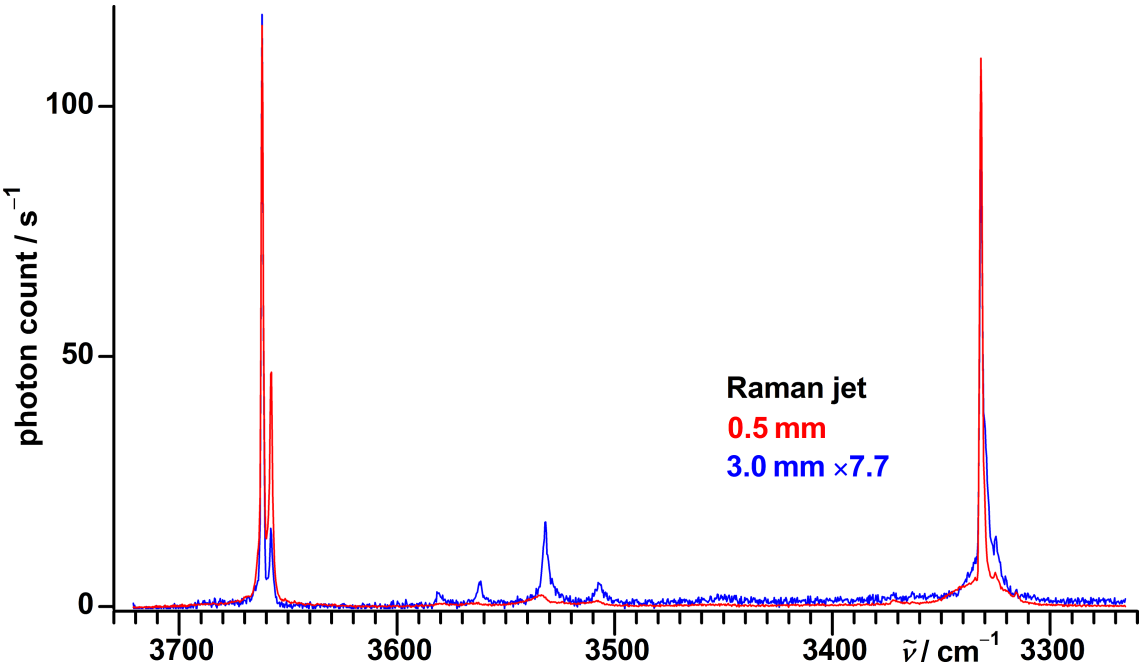

Figure S21: Extended range Raman jet spectra of propargyl alcohol at two detection distances from the nozzle scaled to similar intensities of the 3662 cm^{-1} signal.

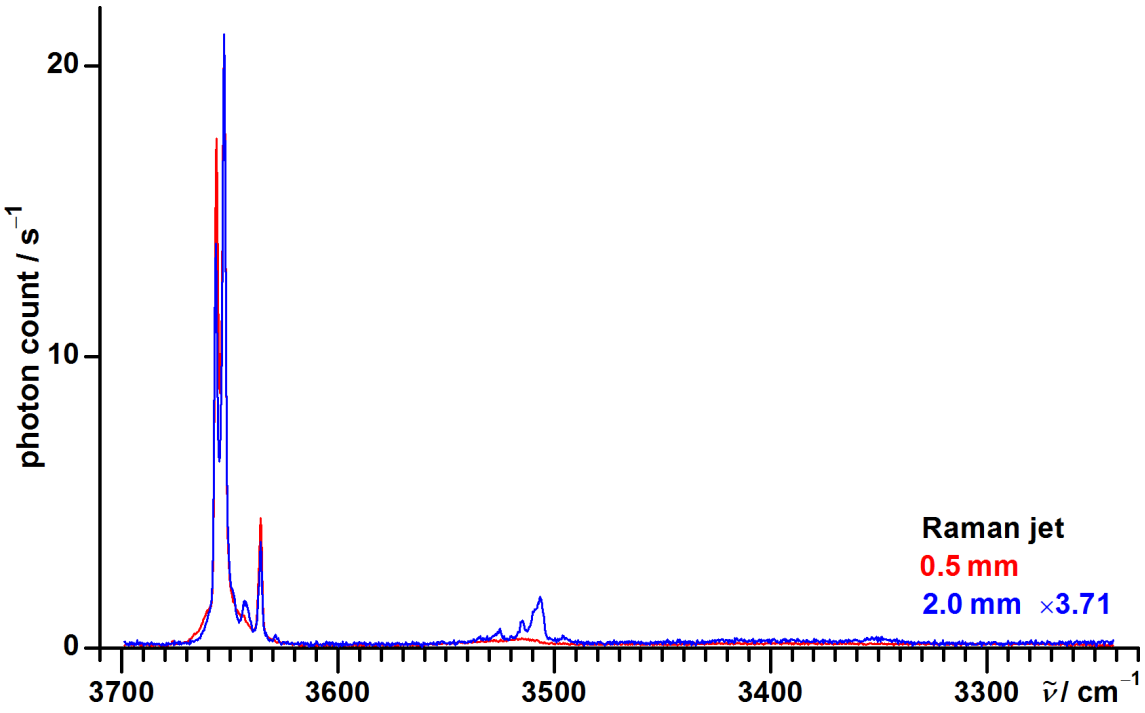

Figure S22: Extended range Raman jet spectra[4] of cyclohexanol at two detection distances from the nozzle scaled to similar intensities of the 3653 cm^{-1} signal.

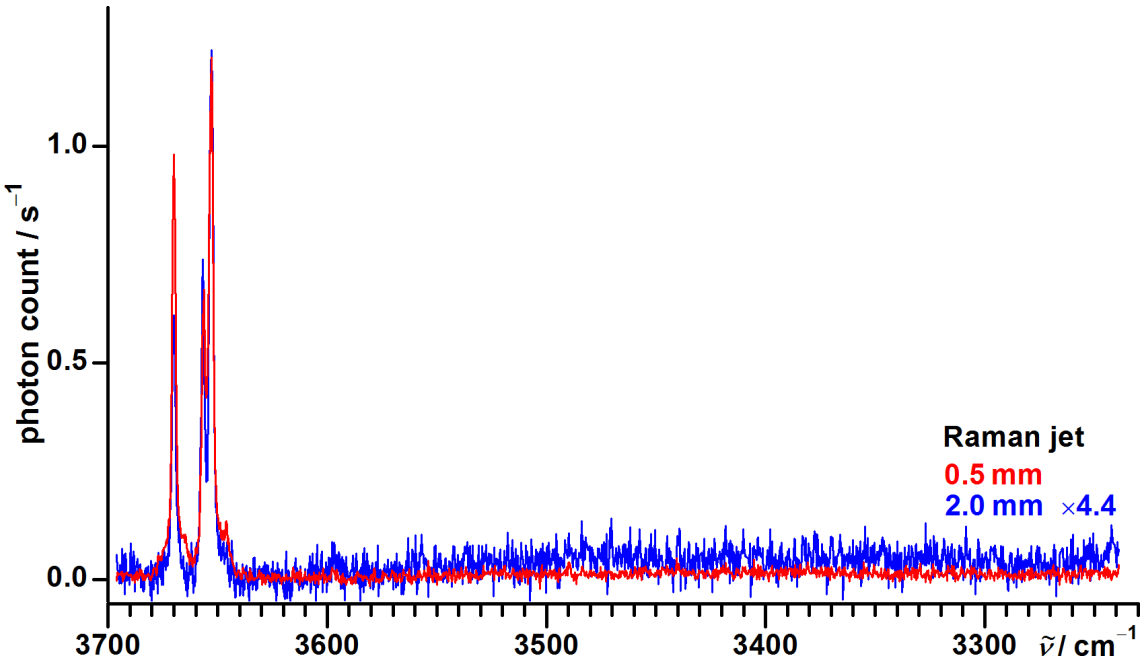

Figure S23: Extended range Raman jet spectra of (−)-borneol at two detection distances from the nozzle scaled to the similar intensities of the 3653 cm^{-1} signal.

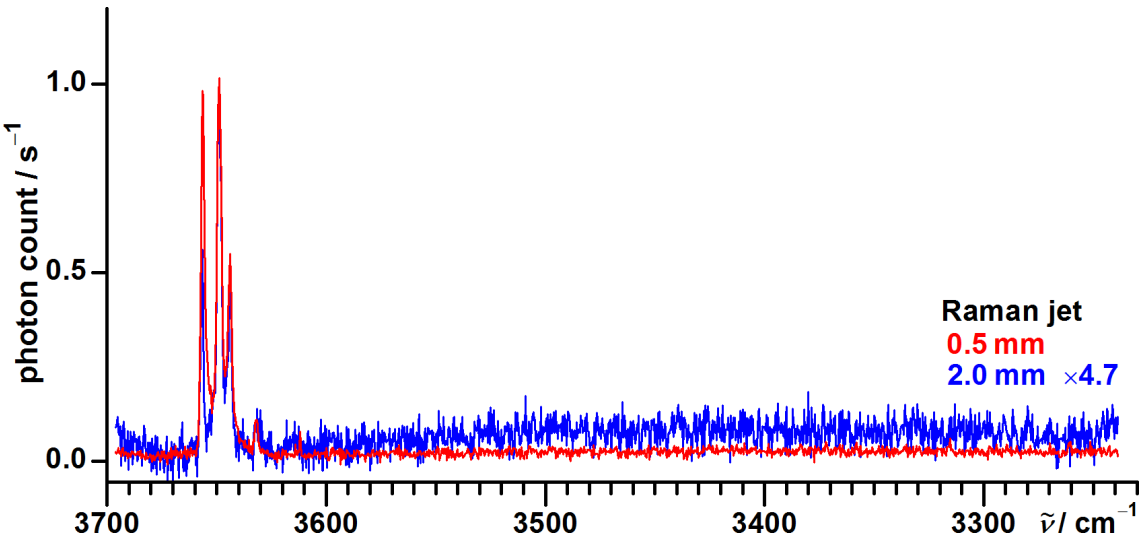

Figure S24: Extended range Raman jet spectra of (−)-isopinocampheol at two detection distances from the nozzle scaled to similar intensities of the 3649 cm^{-1} signal.

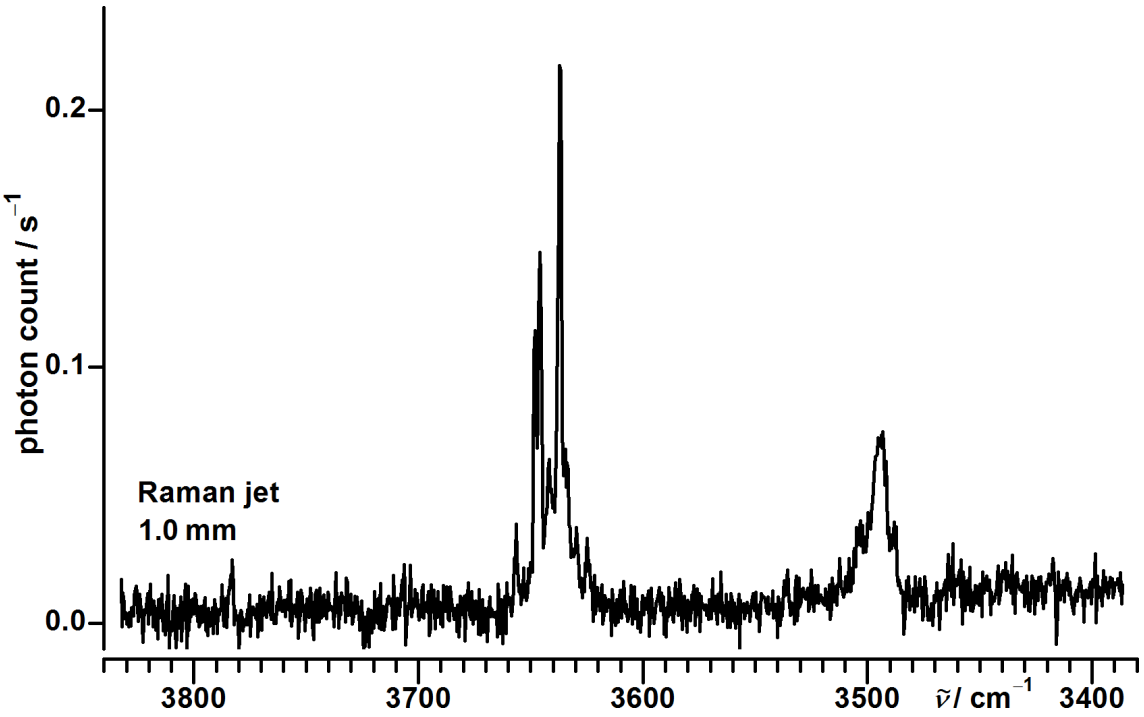

Figure S25: Extended range Raman jet spectrum of 2-methyl-2-butanol.

13 Evaluation of additional alcohols outside the data set

13.1 Evaluation of 1-octanol

1-Octanol has a rich conformational diversity which can be described by five CCCC, one CCCO and one CCOH dihedral. In an FTIR jet study[25,54] a single band at 3680 cm^{-1} was observed. A *trans* arrangement was concluded for the CCOH dihedral and tentatively for the other dihedrals as well, on the basis of exploratory MP2/6-311+G* calculations. In Ref. 54 it was mentioned, however, that a *gauche* arrangement for the CCCO dihedral might also be plausible in the light of (at that time) new results[55] for *n*-alkanols with shorter carbon chains. These two conformers in question are shown in Fig. 26.

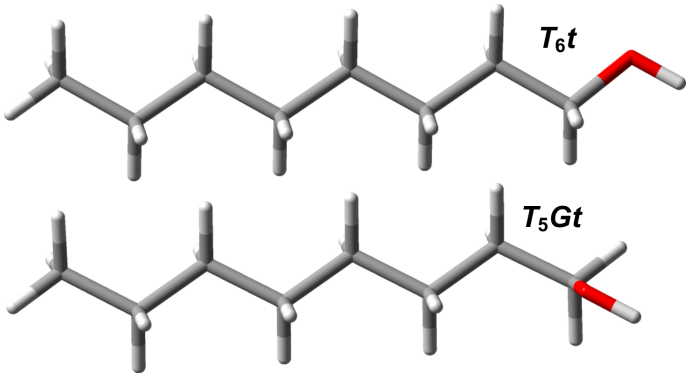

Figure S26: Two conformers of 1-octanol optimized at B3LYP-D3 level.

Our model supports the T_5Gt conformational assigmnent, with predictions within $\pm 1\,cm^{-1}$ of the observed band position, while deviations for the fully stretched T_6t conformer are slightly larger (Table S28).

Table S28: Experimental band position and deviations of the predictions for the OH-stretching fundamentals of conformers of 1-octanol

conformer	method	$\tilde{\nu}/\,cm^{-1}$	$(\omega + \kappa - \tilde{\nu}_{exp})/\,cm^{-1}$
?	experiment	3680	
T_5Gt	B3LYP-D3	3679	−1
T_5Gt	PBE0-D3	3681	1
T_5Gt	SCS-LMP2	3681	1
T_6t	B3LYP-D3	3675	−5
T_6t	PBE0-D3	3677	−3
T_6t	SCS-LMP2	3678	−2

This is further supported on the intensity side by the enantiomeric degeneracy, predicted lower energy and higher IR band strength of T_5Gt (Table S29).

Table S29: Calculated relative zero-point-corrected energies and IR band strengths of the OH-stretching fundamentals for conformers of 1-octanol

conformer	method	$E^0_{rel}/\,kJ\,mol^{-1}$	$I/\,km\,mol^{-1}$
T_5Gt	B3LYP-D3	0	33
T_5Gt	PBE0-D3	0	39
T_5Gt	SCS-LMP2	0	35
T_6t	B3LYP-D3	0.2	30
T_6t	PBE0-D3	0.2	36
T_6t	SCS-LMP2	0.3	33

13.2 Evaluation of 2,3,3-trimethylbutan-2-ol

For 2,3,3-trimethylbutan-2-ol a degenerate g and a non-degenerate t conformer regarding the HOCC dihedral can be expected (Fig. 27).

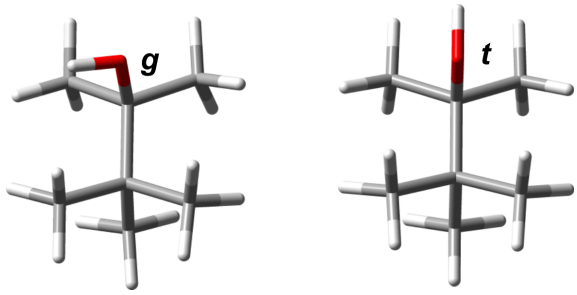

Figure S27: Conformers of 2,3,3-trimethylbutan-2-ol optimized at B3LYP-D3 level.

In an FTIR jet and gas phase study[56–58] a single band at 3650 cm^{-1} was observed, which was later tentatively assigned to the g conformer.[25] The different underlying methods in our model make conflicting predictions. At B3LYP-D3 level a t assignment is strongly encouraged, at SCS-LMP2 level instead a g assignment seems more likely, while at PBE0-D3 level a spectral conincidence of both conformers is predicted (Table S30). The predicted energetic difference between both conformers is also quite method dependent (Table S31).

Table S30: Experimental band position and deviations of the predictions for the OH-stretching fundamentals of conformers of 2,3,3-trimethylbutan-2-ol

conformer	method	$\tilde{\nu}/\,\mathrm{cm}^{-1}$	$(\omega+\kappa-\tilde{\nu}_{\mathrm{exp}})/\,\mathrm{cm}^{-1}$
?	experiment	3650	
g	B3LYP-D3	3657	7
g	PBE0-D3	3651	1
g	SCS-LMP2	3653	3
t	B3LYP-D3	3651	1
t	PBE0-D3	3650	0
t	SCS-LMP2	3644	−6

Table S31: Calculated relative zero-point-corrected energies and IR band strengths of the OH-stretching fundamentals for conformers of 2,3,3-trimethylbutan-2-ol

conformer	method	$E^0_{\mathrm{rel}}/\,\mathrm{kJ\,mol}^{-1}$	$I/\,\mathrm{km\,mol}^{-1}$
g	B3LYP-D3	0.3	16
g	PBE0-D3	−0.04	18
g	SCS-LMP2	0.8	19
t	B3LYP-D3	0	15
t	PBE0-D3	0	18
t	SCS-LMP2	0	18

In the FTIR spectrum of the stationary gas phase at room temperature a symmetric band also centered at 3650 cm^{-1} is observed, provding no hint for the second conformer. This makes the PBE0-D3 prediction – a conincidence within the used spectral resolution (2 cm^{-1}) – the most likely interpretation. This would be in line with the structurally related Gg_{het} and Gt conformers of 2-methyl-2-butanol, which are only partly resolved by Raman jet spectroscopy and for whose spectral positions B3LYP-D3 and SCS-LMP2 show similar over- and underestimations (Table 6 in the main document).

13.3 Evaluation of tri-*tert*-butylcarbinol

Tri-*tert*-butylcarbinol (3-*tert*-butyl-2,2,4,4-tetramethyl-pentan-3-ol) is a tertiary alcohol, its structural formula and optimized geometry are shown in Fig. 28.

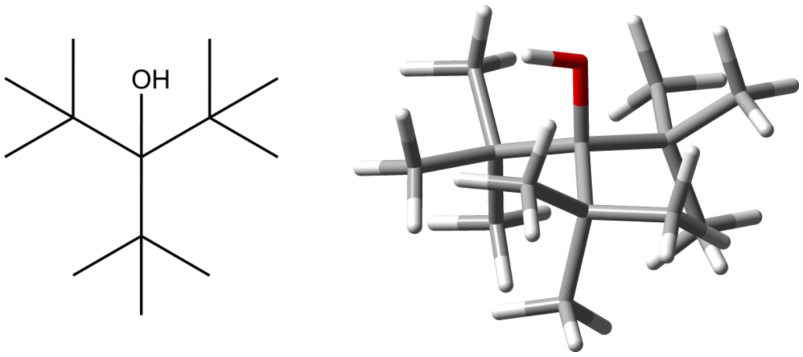

Figure S28: Structural formula and optimized structure of tri-*tert*-butylcarbinol at B3LYP-D3 level.

To reduce the steric conflict between them, the three *tert*-butyl groups are rotated in a sychronized way out of the idealized staggered arrangement and the $C_\alpha - C_\beta$-bonds are strongly elongated (about 1.63 Å compared to 1.53 Å for *tert*-butyl alcohol at B3LYP-D3 level). Expected is a single conformer with enantiomeric degeneracy, resulting from sychronized clockwise or counterclockwise deviation from the staggered arrangement. For the stretching wavenumber of the OH group in this unique chemical environment quite different values are predicted by B3LYP-D3 compared to PBE0-D3 and SCS-LMP2 in our model (Table S32). A reported value of 3651 cm^{-1} for the vapor at 100 °C supports the PBE0-D3 and SCS-LMP2 predictions.[59] However, this should be verified under jet expansion conditions with reduced thermal excitation.

Table S32: Experimental band position and deviations of the predictions for the OH-stretching fundamental of tri-*tert*-butylcarbinol

method	$\tilde{\nu}$/ cm^{-1}	$(\omega + \kappa - \tilde{\nu}_{exp})$/ cm^{-1}
FTIR vapor	3651 [59]	
B3LYP-D3	3663	12
PBE0-D3	3648	−3
SCS-LMP2	3650	−1

14 Calculation of Raman cross sections

In a first step the Raman activities A_R and depolarisation ratios P from the Gaussian 09 output are converted into the derivatives of the isotropic and anisotropic polarisability α' and γ' according to eqn 11 and 12.[60]

$$\alpha'^2 = \frac{A_\mathrm{R}}{45}\left(1 - \frac{7P}{3P+3}\right) \tag{11}$$

$$\gamma'^2 = \frac{A_\mathrm{R}P}{3P+3} \tag{12}$$

Detection sensitivity for differently polarised light is accounted for by the empirically determined polynomial in eqn 13 (determined by M. Gawrilow, Ref. 51). For $\tilde{\nu}$ the corrected harmonic values are used.

$$\begin{aligned} f(\tilde{\nu}) =& 1.7654 \\ &+ 2.6970 \cdot 10^{-10}\,\mathrm{cm}^3 \cdot (\tilde{\nu} - 2000\,\mathrm{cm}^{-1})^3 \\ &+ 0.4316 \cdot 10^{-13}\,\mathrm{cm}^4 \cdot (\tilde{\nu} - 2000\,\mathrm{cm}^{-1})^4 \\ &- 1.1285 \cdot 10^{-16}\,\mathrm{cm}^5 \cdot (\tilde{\nu} - 2000\,\mathrm{cm}^{-1})^5 \\ &- 0.1278 \cdot 10^{-19}\,\mathrm{cm}^6 \cdot (\tilde{\nu} - 2000\,\mathrm{cm}^{-1})^6 \\ &+ 0.1926 \cdot 10^{-22}\,\mathrm{cm}^7 \cdot (\tilde{\nu} - 2000\,\mathrm{cm}^{-1})^7 \\ &+ 0.1029 \cdot 10^{-26}\,\mathrm{cm}^8 \cdot (\tilde{\nu} - 2000\,\mathrm{cm}^{-1})^8 \\ &- 1.1527 \cdot 10^{-30}\,\mathrm{cm}^9 \cdot (\tilde{\nu} - 2000\,\mathrm{cm}^{-1})^9 \end{aligned} \tag{13}$$

Raman cross sections $\sigma(\tilde{\nu})$ are finally obtained through eqn 14, using the laser wavelength $\lambda_\mathrm{Laser} = 532.27$ nm.

$$\sigma(\tilde{\nu}) = \frac{2\pi^2 h \lambda_\mathrm{Laser}^{-1}}{45c} \cdot \frac{\left(\lambda_\mathrm{Laser}^{-1} - \tilde{\nu}\right)^3}{\tilde{\nu}} \cdot \left(45\alpha'^2 + 4\gamma'^2 + \frac{3\gamma'^2}{f(\tilde{\nu})}\right) \tag{14}$$

References

[1] C. A. Stortz, *J. Phys. Org. Chem.*, 2010, **23**, 1173–1186.

[2] M. Juanes, I. Usabiaga, I. León, L. Evangelisti, J. A. Fernández and A. Lesarri, *Angew. Chem. Int. Ed.*, 2020, **59**, 14081–14085.

[3] M. Juanes, W. Li, L. Spada, L. Evangelisti, A. Lesarri and W. Caminati, *Phys. Chem. Chem. Phys.*, 2019, **21**, 3676–3682.

[4] B. Hartwig, *Ramanspektroskopie zur Konformation und Aggregation von Cyclohexanderivaten*, master's thesis, Georg-August-Universität Göttingen, 2018.

[5] J. Caballero and J. Van Der Maas, *J. Mol. Struct.*, 1986, **147**, 231–242.

[6] G. Avila, J. Fernández, G. Tejeda and S. Montero, *J. Mol. Spectrosc.*, 2004, **228**, 38–65.

[7] I. León, R. Montero, A. Longarte and J. A. Fernández, *J. Chem. Phys.*, 2013, **139**, 174312.

[8] E. F. Weigand and H.-J. Schneider, *Org. Magn. Reson.*, 1979, **12**, 637–644.

[9] R. Medel, C. Stelbrink and M. A. Suhm, *Angew. Chem. Int. Ed.*, 2019, **58**, 8177–8181.

[10] R. Medel, *Schwingungsspektroskopische Untersuchungen zur Chiralitätserkennung und Torsionsdynamik bei Alkoholen*, Dissertation, Georg-August-Universität Göttingen, 2020.

[11] J. A. Widegren and T. J. Bruno, *Environ. Sci. Technol.*, 2010, **44**, 388–393.

[12] E. Vogt, P. Bertran Valls and H. G. Kjaergaard, *J. Phys. Chem. A*, 2020, **124**, 932–942.

[13] K. Takahashi, M. Sugawara and S. Yabushita, *J. Phys. Chem. A*, 2003, **107**, 11092–11101.

[14] J. Altnöder, S. Oswald and M. A. Suhm, *J. Phys. Chem. A*, 2014, **118**, 3266–3279.

[15] T. N. Wassermann and M. A. Suhm, *J. Phys. Chem. A*, 2010, **114**, 8223–8233.

[16] F. Kollipost, K. Papendorf, Y.-F. Lee, Y.-P. Lee and M. A. Suhm, *Phys. Chem. Chem. Phys.*, 2014, **16**, 15948–15956.

[17] F. Kollipost, *Schwingungsdynamik in O–H···O-verbrückten Aggregaten: FTIR-Spektroskopie vom Nah- bis zum Ferninfraroten*, Dissertation, Georg-August-Universität Göttingen, 2015.

[18] Y. J. Hu, H. B. Fu and E. R. Bernstein, *J. Chem. Phys.*, 2006, **125**, 154305.

[19] M. Mons, E. G. Robertson, L. C. Snoek and J. P. Simons, *Chem. Phys. Lett.*, 1999, **310**, 423–432.

[20] M. Mons, E. G. Robertson and J. P. Simons, *J. Phys. Chem. A*, 2000, **104**, 1430–1437.

[21] R. Medel and M. A. Suhm, *Phys. Chem. Chem. Phys.*, 2020, **22**, 25538–25551.

[22] B. J. Miller, H. G. Kjaergaard, K. Hattori, S.-i. Ishiuchi and M. Fujii, *Chem. Phys. Lett.*, 2008, **466**, 21–26.

[23] N. Guchhait, T. Ebata and N. Mikami, *J. Am. Chem. Soc.*, 1999, **121**, 5705–5711.

[24] T. N. Wassermann, M. A. Suhm, P. Roubin and S. Coussan, *J. Mol. Struct.*, 2012, **1025**, 20–32.

[25] C. Cézard, C. A. Rice and M. A. Suhm, *J. Phys. Chem. A*, 2006, **110**, 9839–9848.

[26] J. Altnöder, A. Bouchet, J. J. Lee, K. E. Otto, M. A. Suhm and A. Zehnacker-Rentien, *Phys. Chem. Chem. Phys.*, 2013, **15**, 10167.

[27] A. Bouchet, J. Altnöder, M. Broquier and A. Zehnacker, *J. Mol. Struct.*, 2014, **1076**, 344–351.

[28] K. Le Barbu-Debus, F. Lahmani, A. Zehnacker-Rentien, N. Guchhait, S. S. Panja and T. Chakraborty, *J. Chem. Phys.*, 2006, **125**, 174305.

[29] M. Albrecht, J. Will and M. A. Suhm, *Angew. Chem.*, 2010, **122**, 6339–6342.

[30] K. Le Barbu-Debus, N. Seurre, F. Lahmani and A. Zehnacker-Rentien, *Phys Chem Chem Phys*, 2002, **4**, 4866–4876.

[31] K. Le Barbu, F. Lahmani, M. Mons, M. Broquier and A. Zehnacker, *Phys. Chem. Chem. Phys.*, 2001, **3**, 4684–4688.

[32] P. Zielke and M. A. Suhm, *Phys. Chem. Chem. Phys.*, 2006, **8**, 2826–2830.

[33] H. Schaal, T. Häber and M. A. Suhm, *J. Phys. Chem. A*, 2000, **104**, 265–274.

[34] P. Zielke, *Ramanstreuung am Überschallstrahl: Wasserstoffbrückendynamik aus neuer Perspektive*, Dissertation, Georg-August-Universität Göttingen, 2007.

[35] S. Oswald, M. Wallrabe and M. A. Suhm, *J. Phys. Chem. A*, 2017, **121**, 3411–3422.

[36] M. Heger, *Diagonal and Off-Diagonal Anharmonicity in Hydrogen-Bonded Systems*, Dissertation, Georg-August-Universität-Göttingen, 2016.

[37] R. W. Larsen, P. Zielke and M. A. Suhm, *J. Chem. Phys.*, 2007, **126**, 194307.

[38] H.-L. Han, C. Camacho, H. A. Witek and Y.-P. Lee, *J. Chem. Phys.*, 2011, **134**, 144309.

[39] H. B. Fu, Y. J. Hu and E. R. Bernstein, *J. Chem. Phys.*, 2006, **124**, 024302.

[40] Y. J. Hu, H. B. Fu and E. R. Bernstein, *J. Chem. Phys.*, 2006, **125**, 154306.

[41] M. Heger, R. A. Mata and M. A. Suhm, *Chem. Sci.*, 2015, **6**, 3738–3745.

[42] T. Scharge, D. Luckhaus and M. A. Suhm, *Chem. Phys.*, 2008, **346**, 167–175.

[43] M. A. Suhm and F. Kollipost, *Phys. Chem. Chem. Phys.*, 2013, **15**, 10702.

[44] T. Scharge, T. N. Wassermann and M. A. Suhm, *Z. Für Phys. Chem.*, 2008, **222**, 1407–1452.

[45] Y. Liu, C. A. Rice and M. A. Suhm, *Can. J. Chem.*, 2004, **82**, 1006–1012.

[46] B. Hartwig, M. Lange, A. Poblotzki, R. Medel, A. Zehnacker and M. A. Suhm, *Phys. Chem. Chem. Phys.*, 2020, **22**, 1122–1136.

[47] A. Sharma, I. Reva, R. Fausto, S. Hesse, Z. Xue, M. A. Suhm, S. K. Nayak, R. Sathishkumar, R. Pal and T. N. Guru Row, *J. Am. Chem. Soc.*, 2011, **133**, 20194–20207.

[48] J. Altnöder, J. J. Lee, K. E. Otto and M. A. Suhm, *ChemistryOpen*, 2012, **1**, 269–275.

[49] A. Nejad, E. Meyer and M. A. Suhm, *J Phys Chem Lett*, 2020, **11**, 5228–5233.

[50] M. Heger, M. A. Suhm and R. A. Mata, *J. Chem. Phys.*, 2014, **141**, 101105.

[51] M. Gawrilow and M. A. Suhm, *Phys. Chem. Chem. Phys.*, 2020, **22**, 15303–15311.

[52] M. Heger, K. E. Otto, R. A. Mata and M. A. Suhm, *Phys. Chem. Chem. Phys.*, 2015, **17**, 9899–9909.

[53] S. Oswald and M. A. Suhm, *Angew. Chem. Int. Ed.*, 2017, **56**, 12672–12676.

[54] C. A. Rice, *Jet-FTIR spectroscopy of biomolecular model systems*, Dissertation, Georg-August-Universität Göttingen, 2007.

[55] T. N. Wassermann, P. Zielke, J. J. Lee, C. Cézard and M. A. Suhm, *J. Phys. Chem. A*, 2007, **111**, 7437–7448.

[56] T. Häber, U. Schmitt and M. A. Suhm, *Phys. Chem. Chem. Phys.*, 1999, **1**, 5573–5582.

[57] T. Häber, *Ragout-Jet-FTIR-Spektroskopie: Eine neuartige Methode zur Untersuchung der Dyamik von Oligomeren und nanometer-großen Molekülclustern*, Dissertation, Georg-August-Universität Göttingen, 2000.

[58] D. Zimmermann, *Überschallstrahlmessungen und quantenchemische Rechungen zur Aggregation sterisch anspruchsvoller Alkohole*, diploma thesis, unpublished, Georg-August-Universität Göttingen, 2000.

[59] J. Caballero, C. Bruynes and J. Van Der Maas, *J. Mol. Struct.*, 1986, **147**, 243–253.

[60] N. O. B. Lüttschwager, *Raman Spectroscopy of Conformational Rearrangements at Low Temperatures Folding and Stretching of Alkanes in Supersonic Jets*, Springer International Publishing, Cham, 2014.